

TacMan-Turbo: Proactive Tactile Control for Robust and Efficient Articulated Object Manipulation

Zihang Zhao^{a,b}, Zhenghao Qi^a, Yuyang Li^a, Leiyao Cui^{a,c}, Zhi Han^{c,*}, Lecheng Ruan^{d,*}, Yixin Zhu^{a,e,f,*}

^aInstitute for Artificial Intelligence, Peking University

^bLeapZenith AI Research

^cUniversity of Chinese Academy of Sciences

^dCollege of Engineering, Peking University

^eSchool of Psychological and Cognitive Sciences, Peking University

^fBeijing Key Laboratory of Behavior and Mental Health, Peking University

Abstract

Adept manipulation of articulated objects is essential for robots to operate successfully in human environments. Such manipulation requires both effectiveness—reliable operation despite uncertain object structures—and efficiency—swift execution with minimal redundant steps and smooth actions. Existing approaches struggle to achieve both objectives simultaneously: methods relying on predefined kinematic models lack effectiveness when encountering structural variations, while the tactile-informed approach achieves robust manipulation without kinematic priors but compromises efficiency through reactive, step-by-step exploration-compensation cycles. This paper introduces TacMan-Turbo, a novel proactive tactile control framework for articulated object manipulation that resolves this fundamental trade-off. Unlike previous approaches that treat tactile contact deviations merely as error signals requiring compensation, our method interprets these deviations as rich sources of local kinematic information. This new perspective enables our controller to predict optimal future interactions and make proactive adjustments, significantly enhancing manipulation efficiency. In comprehensive evaluations across 200 diverse simulated articulated objects and real-world experiments, our approach maintains a 100% success rate while significantly outperforming the previous tactile-informed method in time efficiency, action efficiency, and trajectory smoothness (all p-values < 0.0001). These results demonstrate that the long-standing trade-off between effectiveness and efficiency in articulated object manipulation can be successfully resolved without relying on prior kinematic knowledge. Our findings reveal that tactile feedback serves a dual purpose: providing not only error signals for reactive control but also critical structural information that enables proactive control. By enabling robots to manipulate articulated objects both reliably and efficiently, this work advances robot capabilities for seamless operation in dynamic, human-centric environments.

Keywords: Contact control, contact sensing, manipulation of articulated objects, and efficient manipulation.

1. Introduction

Adept manipulation of articulated objects, from doors and drawers to various household items, constitutes one of the basic capabilities that robots must master to function effectively in human-centric environments [54]. Success in this domain hinges on two critical objectives: *effectiveness*—the reliable manipulation of objects despite uncertain internal structures, and *efficiency*—the execution of tasks with minimal redundant movements and smooth trajectories [24, 23].

Current approaches struggle to achieve both objectives simultaneously. Methods that rely on pre-provided kinematic information demonstrate efficiency in controlled scenarios but often fail when encountering discrepancies between assumed and actual object kinematics. Conversely, while the recent

tactile-informed approach by Zhao *et al.* [73] successfully achieves robust manipulation despite kinematic uncertainty, it sacrifices efficiency—requiring several minutes to manipulate a single object due to its cautious, step-by-step exploration-compensation mechanism. This fundamental trade-off between effectiveness and efficiency remains unresolved in articulated object manipulation, as further detailed in Section 2.1.

To address this challenge, we propose TacMan-Turbo, a novel proactive control framework that fundamentally reimagines how tactile feedback can guide manipulation. While acknowledging Zhao *et al.*'s insight [73] in using robot-object contact deviations as state representations, TacMan-Turbo interprets these tactile-informed deviations in a different manner—not just as position errors requiring compensation, but as rich sources of information indicating the object's local kinematics. By systematically collecting sequences of these observations, TacMan-Turbo enables accurate prediction of subsequent interaction positions with local optimality. This predictive capability allows the controller to make **proactive** adjustments rather than relying solely on **reactive** corrections,

*Corresponding author

Email addresses: hanzhi@sia.cn (Zhi Han), ruanlecheng@uc1a.edu (Lecheng Ruan), yixin.zhu@uc1a.edu (Yixin Zhu)

¹Zihang Zhao and Zhenghao Qi contributed equally to this work.

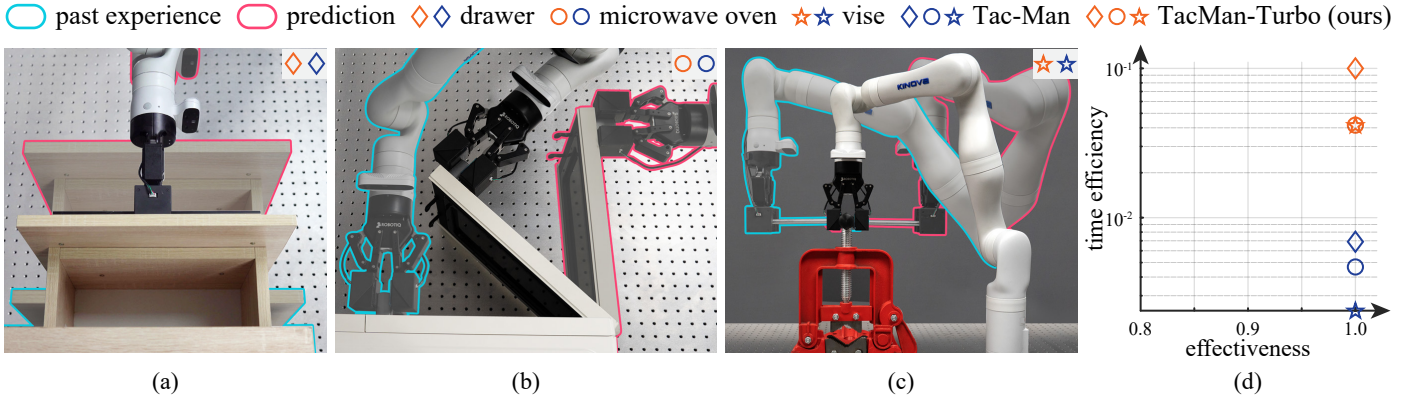


Figure 1: **Robust and efficient tactile-informed manipulation of articulated objects.** TacMan-Turbo enables robots to achieve both effective and efficient manipulation of articulated objects through a novel tactile-based control framework. Unlike previous approaches, TacMan-Turbo leverages past tactile experience to extract local kinematic information, allowing the controller to predict optimal interaction positions and make proactive adjustments—all without requiring pre-provided object kinematics. This capability significantly enhances manipulation efficiency while maintaining robustness across diverse scenarios. Panels (a-c) demonstrate TacMan-Turbo’s versatility across various joint mechanisms: (a) manipulating a prismatic-joint drawer in just 10 seconds, (b) operating a revolute-joint microwave oven in 24 seconds, and (c) controlling a complex vise with a helical handle path in 24 seconds. Panel (d) quantifies these improvements, showing that while maintaining 100% effectiveness, our method achieves approximately 15 \times , 11 \times , and 18 \times higher time efficiency than the recent tactile-informed method, Tac-Man [73], as measured by average manipulation speeds. These order-of-magnitude improvements in efficiency without compromising reliability effectively resolve the longstanding trade-off between effectiveness and efficiency in articulated object manipulation.

thereby significantly improving manipulation efficiency while maintaining robustness. As illustrated in Fig. 1, this novel approach preserves the effectiveness of contact-based manipulation while enabling substantially more efficient execution.

We validate TacMan-Turbo through comprehensive evaluations in both simulation and real-world settings. Our test scenarios systematically cover articulated objects with diverse joint types—from basic prismatic and revolute joints to complex mechanisms involving concurrent translational and rotational movements. Across 200 simulated articulated objects and multiple real-world experiments, TacMan-Turbo achieves the same perfect manipulation success rate as the previous tactile-informed approach while significantly improving all efficiency metrics: time efficiency, action efficiency, and trajectory smoothness (all comparisons yielding p-values < 0.0001). These results confirm that TacMan-Turbo successfully mitigates the long-standing effectiveness-efficiency trade-off in articulated object manipulation.

This paper makes two major contributions:

- We introduce TacMan-Turbo, a novel proactive tactile control framework that effectively resolves the trade-off between efficiency and effectiveness in articulated object manipulation. While traditional approaches treat contact deviations solely as error signals requiring compensation, TacMan-Turbo extracts valuable kinematic information from these deviations to enable proactive adjustments through robust tactile-informed predictive control. This paradigm shift significantly enhances manipulation efficiency while maintaining effectiveness and eliminating reliance on pre-provided object kinematics—data that is often imprecise or unavailable in dynamic, human-centric environments.
- Through extensive evaluation across 200 diverse articulated objects in simulation and multiple real-world experiments, we demonstrate TacMan-Turbo’s ability to achieve 100% ma-

nipulation success rate while significantly improving all efficiency metrics—time consumption, action efficiency, and trajectory smoothness—regardless of joint configurations or kinematic complexities. Our comprehensive real-world validation confirms that this enhanced efficiency occurs without compromising manipulation reliability, representing a meaningful advancement toward practical robot deployment in human environments.

The remainder of this paper is organized as follows: Section 2 positions our work within the broader context of robotic manipulation research. Section 3 presents the theoretical framework and implementation details of TacMan-Turbo. Sections 4 and 5 evaluate TacMan-Turbo through simulation studies and real-world experiments, respectively. Section 6 analyzes TacMan-Turbo’s performance characteristics and discusses future research directions. Finally, Section 7 summarizes our findings and contributions.

2. Related Work

This section contextualizes TacMan-Turbo’s contributions within the broader landscape of robotic research. We begin by assessing current approaches to articulated object manipulation, establishing the fundamental trade-off between effectiveness and efficiency that motivates our work (Section 2.1). In Section 2.2, we explore contact modeling techniques, highlighting how the proposed method builds upon and advances previous work to address the effectiveness-efficiency trade-off. Next, Section 2.3 examines contact sensing technologies, categorizing them into force-based and geometry-based approaches while explaining their compatibility with our method. Finally, Section 2.4 reviews contact control strategies, tracing their evolution from early reactive feedback systems to our proposed proactive tactile control frameworks.

2.1. Articulated Object Manipulation

Approaches to articulated object manipulation can be categorized based on their strategies for addressing the fundamental challenges of effectiveness and efficiency. Traditional methods rely on predefined kinematic models provided manually [9, 5]. While these approaches enable efficient manipulation through precise motion planning in controlled environments, they significantly restrict system autonomy by requiring accurate prior knowledge of object kinematics—limiting their effectiveness in real-world scenarios where such information is often unavailable or inaccurate.

To overcome this dependency on manually provided information, subsequent research has focused on the autonomous acquisition of object kinematics. A prominent line of work leverages visual perception to infer kinematic models through geometric reasoning and motion analysis [20, 29, 68, 40, 10, 34, 44]. However, visual information alone often proves insufficient, as visually similar objects may possess fundamentally different internal mechanisms [75, 68, 73]. This inherent limitation has led researchers to integrate additional sensing modalities to resolve ambiguity. By combining multi-frame analysis with wrist-mounted force/torque sensors, more accurate parameter estimation of kinematic models becomes possible through active interaction [24, 19, 23, 39, 36, 31]. Nevertheless, these methods remain constrained by their underlying assumption that objects conform to predefined joint types (*e.g.*, revolute, prismatic), limiting their effectiveness when encountering complex or unconventional mechanisms.

The persistent challenges in model-based approaches have driven the development of learning-based techniques for articulated object manipulation. Imitation learning enables robots to acquire implicit manipulation strategies from human demonstrations, typically facilitated through teleoperation systems [45, 57, 61, 17, 70, 59, 47, 14]. This approach naturally captures human manipulation expertise but faces significant challenges in collecting sufficiently diverse and high-quality demonstration datasets [74]. While transfer learning techniques have improved generalization to similar objects [46, 52], extending these methods to handle arbitrary articulated objects remains challenging due to the vast diversity of possible kinematic structures.

Reinforcement learning offers an alternative paradigm that attempts to overcome the data collection bottleneck by developing manipulation strategies through repeated interactions in simulated environments [53, 62, 7, 15]. This approach has been significantly advanced by the creation of large-scale datasets of articulated objects [41, 60, 33, 16], enabling training across diverse object categories. However, the inevitable sim-to-real gap often leads to degraded performance when these methods are deployed in real-world settings, particularly when encountering previously unseen object variations.

The limitations in both model-based and learning-based approaches recently led to the development of a tactile-informed manipulation framework. Zhao *et al.* [73] introduced a novel approach that achieves reliable manipulation by formulating it as a control problem that compensates for robot-object contact deviations without requiring kinematic priors. While

this method demonstrates remarkable effectiveness in handling unknown articulated objects, its step-by-step exploration-compensation process results in significant time overhead that limits practical deployment. Our work, TacMan-Turbo, advances this foundation by extracting structural information from tactile feedback to enable predictive control. This proactive approach significantly improves manipulation efficiency while maintaining the same level of effectiveness—effectively addressing the long-standing trade-off between these two critical objectives.

2.2. Contact Modeling

Contact modeling has emerged as a fundamental approach in robotics research, providing essential information about robot-environment interactions [50, 30]. The effectiveness of contact-based strategies has been particularly demonstrated in robotic grasping, where accurate contact models enable reliable manipulation across diverse object geometries [4, 32].

Despite its proven success in grasping, contact modeling remains insufficiently explored for articulated object manipulation—a domain with inherently more complex interaction dynamics. Most existing approaches employ simplified contact assumptions, typically modeling fixed contact points between the robot and the object [9, 5, 40, 19, 42, 36, 39]. While this simplification enables efficient computation, it fundamentally fails to capture the dynamic nature of real-world interactions where contact points frequently shift during manipulation. Some progress has been made by relaxing these constraints to permit specific forms of relative motion between the robot and object [24, 23], enabling more effective control command generation. However, these approaches still rely on predefined kinematic models, limiting their effectiveness across diverse object types.

Zhao *et al.* [73] advanced this domain by showing that modeling contact as geometric deviations is sufficient for robust articulated object manipulation without requiring prior kinematic models. While this finding established the power of contact-based approaches, their method’s reactive, step-by-step exploration-compensation mechanism substantially limited its efficiency. Our work, TacMan-Turbo, further advances this direction by extracting local object kinematic information from these contact deviations, enabling proactive adjustments that significantly enhance manipulation efficiency while maintaining the same level of robustness.

2.3. Contact Sensing

The successful implementation of TacMan-Turbo relies on accurate sensing of contacts between robots and objects, leveraging decades of advances in tactile sensing technology [65]. Based on their primary output format, tactile sensors can be categorized into two main types: force-based and geometry-based sensors, each offering distinct advantages for manipulation tasks.

Force-based sensors output contact forces by converting mechanical interactions into electrical signals through various

transduction mechanisms, including conductive fluid [13], resistance [64, 66], capacitance [3, 12], and others. Geometry-based sensors, conversely, directly capture the geometric characteristics of contact interfaces, with vision-based tactile sensors being prominent examples [67, 55, 27, 28, 72].

Since TacMan-Turbo’s core functionality centers on contact geometry modeling for kinematic information extraction, it is naturally compatible with geometry-based sensors that directly provide the required information. Although force-based sensors can also be effectively utilized, they require an additional calibration step using Hooke’s law [18] to convert force measurements into geometric information [73]. To demonstrate TacMan-Turbo’s capabilities, in this paper, we implement our system using the GelSight sensor [67], a well-established geometry-based tactile sensing technology that provides sufficient geometric information about contact surfaces.

2.4. Contact Control

Contact control, also known as tactile control, has evolved into a powerful strategy for robotic manipulation by modulating robot motion based on real-time tactile feedback. This approach was pioneered by Weiss *et al.* [56] and subsequently advanced by Berger and Khosla [2], who provided the first practical implementation demonstrating its potential for precise interaction tasks.

The fundamental challenge in tactile control lies in designing algorithms capable of effectively transitioning from current tactile observations to desired reference states. To address this challenge, researchers have developed two primary approaches: feedback control and direct mapping. Feedback control employs various controllers (*e.g.*, PID controllers) to systematically minimize the difference between observed and desired tactile features, requiring careful selection of task-specific control parameters [26, 22, 25, 49, 35]. Direct mapping, on the contrary, transforms tactile feature differences directly into robot motion commands without explicit parameter tuning. This approach was first introduced by Chen *et al.* [6], who proposed the concept of an inverse tactile Jacobian for 2D edge tracking using manually designed features. This foundational framework was subsequently refined and extended by numerous researchers, including Zhang *et al.* [69] and Sikka *et al.* [51], who demonstrated its versatility in different manipulation scenarios. More recently, Wilson *et al.* [58] advanced the field by introducing motion primitives for cable rearrangement tasks, providing a structured approach to handle deformable objects. Zhao *et al.* [73] made a contribution to this paradigm through their implementation of contact point registration, demonstrating robust manipulation of articulated objects despite their kinematic complexity.

The latest evolution in tactile control has seen the emergence of predictive frameworks that anticipate future tactile states rather than reacting only to current observations. For example, Xu *et al.* [63] employed learning-based techniques to predict future tactile states for reactive grasping. However, such data-driven approaches often face challenges in generalizing across diverse and dynamic tasks due to their dependence on training data distribution. Our method, TacMan-Turbo, introduces

a training-free predictive control framework that takes advantage of previous sequential tactile information. By systematically extracting local kinematic information from these temporal data, our approach predicts optimal subsequent interactions and enables proactive adjustments, substantially enhancing manipulation efficiency without compromising reliability.

3. The Proactive Tactile Control

At its core, TacMan-Turbo is a novel proactive tactile control framework designed for both effective and efficient manipulation of articulated objects. Unlike **reactive** approaches that respond only to current sensory information, TacMan-Turbo extracts local object kinematic patterns from past contact data to predict optimal subsequent interaction positions. This predictive capability enables proactive adjustments that systematically mitigate contact deviations before they significantly impact manipulation performance.

The development of this framework unfolds through four interconnected components. First, Section 3.1 establishes the essential mathematical notation and preliminaries that provide the foundation for our approach. Building on this mathematical framework, Section 3.2 formally defines the articulated object manipulation problem, specifically addressing the dual optimization objectives of effectiveness and efficiency. Next, Section 3.3 introduces our novel prediction framework that analyzes sequential patterns in contact deviations to forecast articulated object states during manipulation. Finally, Section 3.4 details how these kinematic predictions are translated into optimal gripper velocity adjustments while adhering to the robot’s physical constraints and ensuring consistent contact maintenance.

3.1. Notation

To establish a rigorous foundation for our formulation of effective and efficient manipulation, we define the following mathematical notation:

- \mathbb{R} represents the set of real numbers, with \mathbb{R}^+ denoting non-negative reals. Matrix and vector spaces are denoted as $\mathbb{R}^{m \times n}$ and \mathbb{R}^n respectively. The special orthogonal group $SO(n)$ consists of rotation matrices with determinant 1, while the special Euclidean group $SE(n)$ represents rigid body transformations. Additional sets use calligraphic letters (*e.g.*, \mathcal{C}), with $|\cdot|$ denoting set cardinality.
- Vectors are represented by bold lowercase letters (*e.g.*, $q \in \mathbb{R}^n$), with subscript i indicating the i -th element (*e.g.*, q_i). The velocity vector $u \in \mathbb{R}^6$ specifically combines linear velocities $v = [v_x, v_y, v_z]^T \in \mathbb{R}^3$ and angular velocities $\omega = [\omega_x, \omega_y, \omega_z]^T \in \mathbb{R}^3$, where \cdot^T denotes transpose.
- Matrices use bold uppercase letters (*e.g.*, $M \in \mathbb{R}^{m \times n}$), with m_{ij} denoting the entry at row i and column j . The trace operator is written as $\text{tr}(M)$, and $I_{n \times n}$ represents the n -dimensional identity matrix.
- For relative pose representation between frames $\{i\}$ and $\{j\}$, we use position vector $p_i^j \in \mathbb{R}^3$ and rotation matrix $R_i^j \in SO(3)$. When frame $\{j\}$ is the world frame $\{w\}$, we omit

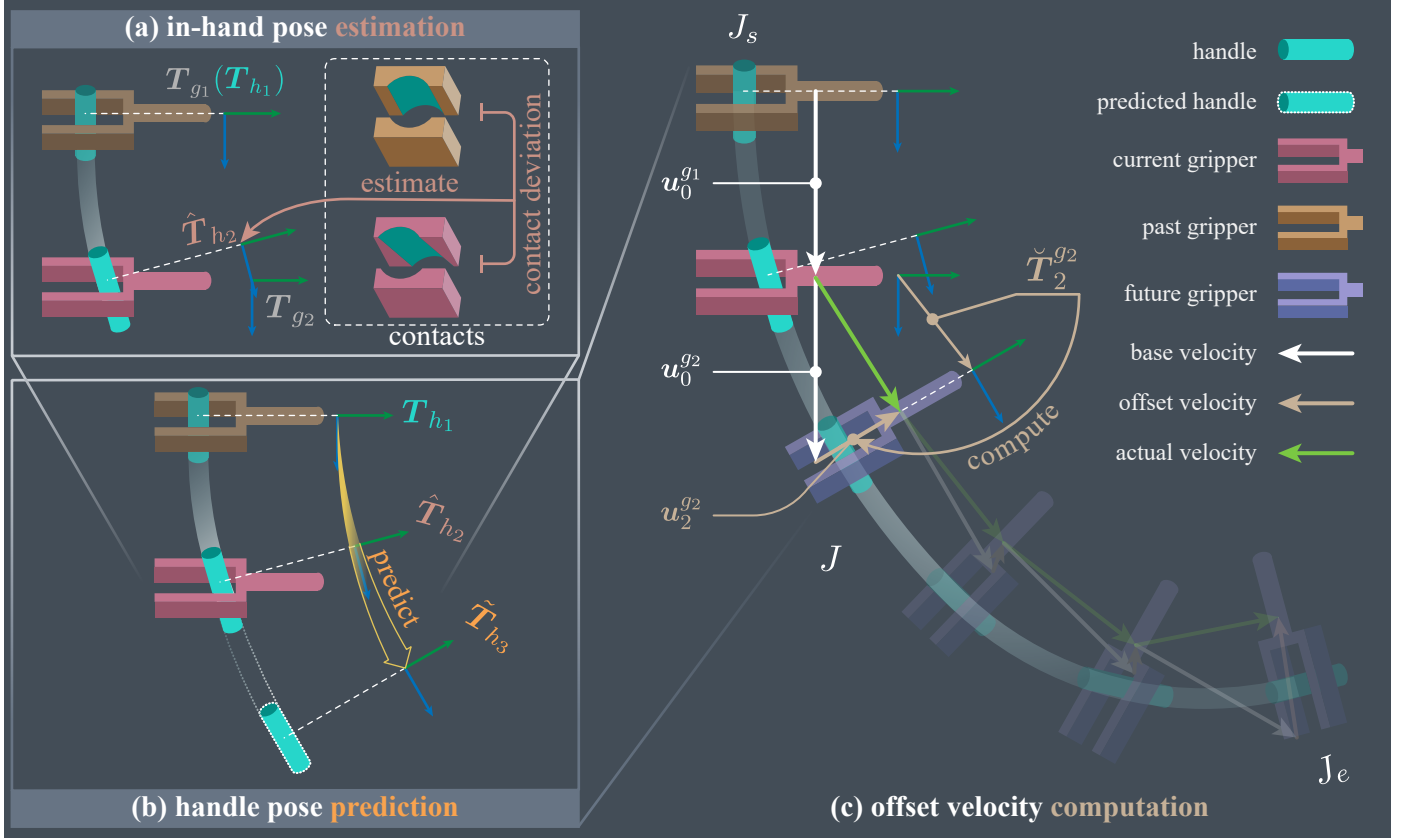


Figure 2: **Schematic overview of proactive tactile proactive control framework, TacMan-Turbo.** Our framework integrates three sequential components that enable proactive manipulation: (a) **In-hand pose estimation** extracts tactile contact patterns from gripper sensors to determine the relative transformation components between current gripper pose T_{g1} and handle pose T_{h1} . (b) **Handle pose prediction** analyzes sequential pose estimates (T_{h1}, T_{h2}) to extract local kinematic patterns, enabling prediction of the future handle pose \hat{T}_{h3} . (c) **Offset velocity computation** generates the optimal control signal by calculating an offset velocity $u_i^{g_i}$ that, when combined with base velocity $u_0^{g_i}$, creates a resultant motion $u_0^{g_i} + u_i^{g_i}$ that aligns future gripper position with predicted handle motion along path J . By proactively adjusting for potential contact deviations, this approach ensures smooth, continuous manipulation from start point J_s to end point J_e without requiring separate correction phases.

the superscript. These components combine into the homogeneous transformation matrix:

$$T_i^j = \begin{bmatrix} R_i^j & p_i^j \\ 0 & 1 \end{bmatrix}.$$

- The unit vector $\hat{w} \in \mathbb{R}^3$ specifies the axis of rotation, defining the direction of rotational motion for articulated objects.

3.2. Problem Formulation

We now formulate the mathematical framework for effective and efficient tactile-informed manipulation of articulated objects. Consider an articulated object with a movable part and its rigidly attached “handle,” as illustrated in Fig. 2. The underlying articulation mechanism constrains the handle’s motion to a 1-DoF trajectory, represented as path J from initial point J_s to target point J_e . In our problem setting, only the initial position J_s is initially known, reflecting real-world scenarios where complete kinematic models are unavailable.

At the start of manipulation, a robot gripper at global pose T_{g1} grasps the handle at pose T_{h1} . For mathematical convenience and without loss of generality, we align the initial handle

coordinate frame with that of the robot gripper:

$$T_{h1} = T_{g1}. \quad (1)$$

The physical interaction between the gripper and handle is characterized by their contact state, denoted by \mathcal{C}_i . This state is represented geometrically as a set containing three-dimensional position vectors of activated contact points in the gripper’s coordinate frame, denoted as $[p_x^{g_i}, p_y^{g_i}, p_z^{g_i}]^T$. Contact points become activated when their normal deformation (illustrated along the x -axis in Fig. 2) exceeds threshold ε :

$$\mathcal{C}_i = \left\{ \left[\begin{array}{c} p_x^{g_i} \\ p_y^{g_i} \\ p_z^{g_i} \end{array} \right] \mid |p_x^{g_i}| \geq \varepsilon \right\}. \quad (2)$$

The initial contact state \mathcal{C}_1 is assumed stable, providing a secure connection without material damage. Generally, any contact state \mathcal{C}_i is defined through a mapping function f_c of handle and gripper poses, as the relative pose between these elements fully determines their interaction:

$$\mathcal{C}_i = f_c(T_{h_i}, T_{g_i}). \quad (3)$$

In practice, this contact state is directly measured by tactile sensors mounted on the gripper.

Manipulation begins with a constant base velocity $u_0^{g_i}$ in the gripper’s coordinate system, aligned with a known rough direction of the manipulation task:

$$u_0^{g_i} = \begin{bmatrix} v_0^{g_i} \\ \omega_0^{g_i} \end{bmatrix}. \quad (4)$$

The acquisition of this base velocity and its impact on manipulation efficiency are examined in detail in Section 6.

Without prior knowledge of the articulation mechanism, the trajectories of the gripper and handle inevitably become misaligned during manipulation. This misalignment produces contact deviations that may result in inefficient or even unstable interactions if not addressed. To mitigate this issue, an offset gripper velocity, denoted as $u_i^{g_i}$, must be introduced to adapt the gripper’s motion to the handle’s constrained path.

The key challenge lies in determining this offset velocity. Efficiency considerations preclude simply halting motion to correct current contact deviations—instead, corrections must be planned proactively for subsequent steps, requiring anticipation of how the contact state will evolve. Therefore, the offset velocity cannot simply react to current deviations but must proactively minimize future contact deviations while maintaining the base velocity. Mathematically, this can be formulated as the following optimization problem:

$$u_i^{g_i} = \arg \min_{u_i^{g_i}} \sum_{(c_1, c_{i+1}) \in \mathcal{K}_{1,i+1}} \|c_1 - c_{i+1}\|_2, \quad (5)$$

where $\mathcal{K}_{1,i+1}$ defines corresponding points between the reference (initial) and subsequent contact states:

$$\mathcal{K}_{1,i+1} = \{(c_1, c_{i+1}) \mid c_1 \in \mathcal{C}_1, c_{i+1} \in \mathcal{C}_{i+1}\}, \quad (6)$$

subject to the velocity limit constraint:

$$u^m \preceq u_0^{g_i} + u_i^{g_i} \preceq u^M, \quad (7)$$

where \preceq denotes an element-wise “less than or equal to” relationship between vectors, while u^m and u^M represent the lower and upper bounds of the velocity that the robot can physically generate.

Given that the contact state depends solely on the poses of the gripper and handle (as established in Eq. (3)), maintaining stable contact requires aligning the gripper’s motion with the handle’s trajectory. Our solution addresses this fundamental challenge in two complementary steps: First, in Section 3.3, we develop a method to predict the handle’s next-step pose $T_{h_{i+1}}$ based on sequential contact patterns observed during interaction. Second, in Section 3.4, we compute the control input $u_i^{g_i}$ that optimally aligns the gripper’s motion with this predicted pose while ensuring compliance with the velocity limit constraints.

3.3. Handle Pose Estimation and Prediction

To enable proactive control adjustments, our approach leverages past contact data to predict the optimal position for subsequent object interactions. This predictive capability builds upon two complementary components: first, estimating current handle poses from observed contact deviations and known gripper poses; second, leveraging the temporal sequence of these estimated poses to predict future handle positions. We begin by detailing our pose estimation approach.

At each time step, the handle pose T_{h_i} relates to the gripper pose T_{g_i} through their relative transformation:

$$T_{h_i} = T_{g_i} T_{h_i}^{g_i}, \quad (8)$$

where $T_{h_i}^{g_i} \in SE(3)$ represents their relative homogeneous transformation. Initially at $i = 1$, $T_{h_1}^{g_1} = I_{4 \times 4}$ following our initial pose definition (Eq. (1)).

For subsequent time steps ($i > 1$), assuming no slip between the sensor outer surface and the handle, any relative transformation can be observed as deviations between the current contact state \mathcal{C}_i and the reference state \mathcal{C}_1 . This relationship enables us to estimate $T_{h_i}^{g_i}$ through the following optimization:

$$\hat{T}_{h_i}^{g_i} = \arg \min_{\hat{T}_{h_i}^{g_i} \in SE(3)} \sum_{(c_1, c_i) \in \mathcal{K}_{1,i}} \left\| \hat{T}_{h_i}^{g_i} \begin{bmatrix} c_1 \\ 1 \end{bmatrix} - \begin{bmatrix} c_i \\ 1 \end{bmatrix} \right\|_2, \quad (9)$$

where

$$\mathcal{K}_{1,i} = \{(c_1, c_i) \mid c_1 \in \mathcal{C}_1, c_i \in \mathcal{C}_i\} \quad (10)$$

defines the corresponding contact point pairs between the reference and current states.

This optimization problem (9) can be efficiently solved using the Kabsch algorithm [21], provided the contact state \mathcal{C}_i satisfies two key constraints:

First, it must contain at least three contact points:

$$|\mathcal{C}_i| \geq 3. \quad (11)$$

Second, these points must be non-collinear. Specifically, there must exist points $p_1, p_2, p_3 \in \mathcal{C}_i$ such that:

$$(p_2 - p_1) \times (p_3 - p_1) \neq 0. \quad (12)$$

Given these constraints, we can estimate the handle pose \hat{T}_{h_i} at each time step i by combining the gripper pose with the estimated relative transformation:

$$\hat{T}_{h_i} = T_{g_i} \hat{T}_{h_i}^{g_i}. \quad (13)$$

Building upon these estimated poses, we now focus on predicting future handle positions. Under the assumptions of smooth object trajectories and sufficiently high sampling frequencies, consecutive handle poses exhibit only slight variations primarily driven by the object’s instantaneous velocity. This makes the constant velocity model—a widely utilized approach across various scenarios, including dynamic ones [11, 43, 48]—particularly effective for such predictions.

Based on this model, the next handle pose $\tilde{T}_{h_{i+1}}$ is predicted as:

$$\tilde{T}_{h_{i+1}} = \hat{T}_{h_i} T_u, \quad (14)$$

where T_u represents the velocity effects, which are assumed to remain constant over short time intervals. Given consistent sampling intervals, T_u is computed from the two most recent pose estimates:

$$T_u = (\hat{T}_{h_{i-1}})^{-1} \hat{T}_{h_i}. \quad (15)$$

While this constant velocity model effectively predicts handle poses, it may introduce minor residual errors relative to ground truth due to the omission of higher-order effects such as acceleration. However, these residual errors are detected by subsequent in-hand pose estimation and corrected during the next prediction step, preventing error accumulation. Moreover, for scenarios involving more dynamic motion or reduced sampling frequencies, this prediction framework can be extended to account for higher-order motion effects by incorporating additional past data—for example, transitioning to a constant acceleration model by using one more observation to account for velocity changes.

As evident from Eq. (15), the proposed constant velocity prediction requires at least two previous observations ($i \geq 2$). For the initial step ($i = 1$), when past data is unavailable, the system relies solely on the base velocity $u_0^{g_i}$ defined in Section 3.2. This integration of pose estimation and prediction provides the foundation for computing appropriate gripper velocities, which we address in the following section.

3.4. Offset Velocity Computation

Having predicted the next handle pose, we now develop a method for computing the offset gripper velocity that proactively compensates for contact deviations while maintaining operational efficiency. In the ideal scenario, the solution is straightforward: align the gripper's next pose precisely with the predicted handle pose to eliminate any potential contact deviation:

$$T_{g_{i+1}} = \tilde{T}_{h_{i+1}}. \quad (16)$$

This desired alignment requires the gripper to execute a specific transformation over a sampling interval $\Delta t \in \mathbb{R}^+$. We compute this required transformation relative to the gripper's current coordinate frame:

$$\tilde{T}_i^{g_i} = \begin{bmatrix} \check{R}_i^{g_i} & \check{p}_i^{g_i} \\ 0 & 1 \end{bmatrix} = (T_{g_i})^{-1} T_{g_{i+1}}. \quad (17)$$

From this transformation, we derive the required velocity components. The linear velocity component $v_i^{g_i}$ of the offset velocity $u_i^{g_i}$ is computed by accounting for both the position difference and the base velocity:

$$v_i^{g_i} = \frac{\check{p}_i^{g_i}}{\Delta t} - v_0^{g_i}. \quad (18)$$

For the angular velocity component $\omega_i^{g_i}$, we employ Ro-

drigues' rotation formula [37]:

$$\omega_i^{g_i} = \hat{\omega}_i^{g_i} \frac{\theta_i}{\Delta t} - \omega_0^{g_i}, \quad (19)$$

where $\theta_i \in [0, \pi]$ represents the rotation angle:

$$\theta_i = \cos^{-1} \left(\frac{1}{2} (\text{tr}(\check{R}_i^{g_i}) - 1) \right), \quad (20)$$

and $\hat{\omega}_i^{g_i} \in \mathbb{R}^3$ denotes the unit vector along the rotation axis, whose computation depends on the rotation angle θ_i . For brevity, the details of this computation are omitted here; interested readers are referred to the comprehensive treatment in [37].

With both linear and angular components determined, we can express the ideal offset velocity:

$$u_i^{g_i} = \begin{bmatrix} v_i^{g_i} \\ \omega_i^{g_i} \end{bmatrix}. \quad (21)$$

While the above formulation provides the theoretically optimal velocity, practical implementation must account for the limitations imposed by robot hardware—specifically the maximum gripper velocities determined by the robot's joint motor limits, as defined in Eq. (7). The relationship between joint velocities $\dot{q}_i \in \mathbb{R}^n$ and the gripper velocity $u_i^{g_i}$ is given by:

$$J(q_i) \dot{q}_i = u_i^{g_i} + u_0^{g_i}, \quad (22)$$

where $J(q_i) \in \mathbb{R}^{6 \times n}$ is the robot Jacobian matrix. For analytical tractability, we assume $n \geq 6$ and that $J(q_i)$ maintains row full rank. Over small time intervals, treating q_i as constant allows us to solve for joint velocities:

$$\dot{q}_i = J^\dagger(q_i) (u_i^{g_i} + u_0^{g_i}), \quad (23)$$

using the pseudoinverse:

$$J^\dagger(q_i) = J(q_i)^\top (J(q_i) J(q_i)^\top)^{-1}. \quad (24)$$

To ensure joint velocities remain within their maximum limits \dot{q}_M , we introduce a scaling factor α :

$$\alpha = \min \left(\min \left(\left\{ \frac{\dot{q}_{M_j}}{\max(|\dot{q}_{ij}|, \varepsilon)} \beta \mid j = 1, \dots, n \right\}, 1 \right), 1 \right), \quad (25)$$

where β is a safety factor and ε represents a small positive constant introduced to prevent division by zero. This scaling yields the final executable offset velocity command:

$$u_i^{g_i} = \begin{bmatrix} \alpha v_i^{g_i} + (\alpha - 1) v_0^{g_i} \\ \alpha \omega_i^{g_i} + (\alpha - 1) \omega_0^{g_i} \end{bmatrix} \quad (26)$$

with the base velocity also scaled by α . Consequently, to achieve the desired handle position $\tilde{T}_{h_{i+1}}$ while respecting joint velocity limits, the execution duration must be adjusted from Δt to:

$$\Delta t' = \frac{\Delta t}{\alpha}. \quad (27)$$

While this scaling may marginally reduce manipulation efficiency, it represents a necessary adjustment to ensure the robot operates within its physical constraints, particularly when addressing large contact deviations that require substantial compensation.

4. Simulation Studies

To thoroughly evaluate TacMan-Turbo, we conducted extensive simulation studies focusing on both manipulation effectiveness and efficiency. This section presents our experimental approach and findings in four parts: we first detail our simulation setup (Section 4.1), establish comparative baselines (Section 4.2), define quantitative evaluation metrics (Section 4.3), and analyze the performance results (Section 4.4).

4.1. Simulation Setup

Our evaluation framework integrates three core components designed to enable comprehensive assessment of manipulation capabilities under controlled yet realistic conditions.

Simulation environment. We implemented our experiments in NVIDIA Isaac Sim, operating at 60 Hz to ensure sufficient temporal resolution for capturing dynamic contact interactions. Critical to our study is the contact simulation method developed by Zhao *et al.* [73], which enables accurate modeling of tactile feedback by monitoring displacement patterns within designated contact regions. This approach captures the nuanced contact dynamics that emerge during the manipulation of articulated objects.

Test articulated objects. To systematically evaluate performance across varying kinematic structures, we assembled a three-category test suite with progressively increasing trajectory complexity:

- 50 objects with prismatic joints from PartNet-Mobility dataset [60] (Fig. 3a), featuring linear motion paths with varying physical characteristics.
- 50 objects with revolute joints also from PartNet-Mobility (Fig. 3b), representing rotational articulations that require continuous adjustment of manipulation direction.
- 100 custom-generated objects with Bézier curve trajectories designed to assess performance on complex, non-linear paths. This category includes 25 curves each of orders 2, 3, 4, and 5, sampled on a 2D plane and constrained to avoid self-intersections. Each curve defines a manipulation path on a 3D playboard, with a toy train positioned at the starting point serving as the handle (Fig. 3c).

Such a design from simple to complex kinematics provides systematic evaluation across a spectrum of trajectory predictability and curvature characteristics. The generation process for the Bézier-based objects followed protocols in Zhao *et al.* [73], producing diverse trajectory complexities that challenge predictive capabilities in distinct ways.

Robot. Our experiments employ a 7-DoF Franka robotic arm, selected for its ability to execute full 6-DoF Cartesian motions—a capability essential for accommodating the diverse movement requirements of our test objects. We also integrate the B* algorithm to place the robot, ensuring that hand trajectories during manipulation remain within the robot workspace [71]. We implement motion control using NVIDIA Isaac Sim’s built-in RMPFlow algorithm [8]. Each experimental trial begins with a standardized initialization: the robot establishes a secure grasp on the target handle, creating a well-defined reference contact state \mathcal{C}_1 that serves as the foundation for subsequent manipulation and deviation measurements.

4.2. Baseline Selection

For comparative analysis, we adopt Tac-Man [73] as our primary baseline, a selection driven by its demonstrated superiority in manipulation effectiveness, outperforming traditional pre-planned methods, impedance control strategies, and learning-based approaches across diverse manipulation scenarios. Since successful task completion is a prerequisite for meaningful efficiency evaluation, we focus our comparative analysis exclusively on methods that reliably satisfy this fundamental criterion.

The key architectural distinction between Tac-Man and our proposed TacMan-Turbo framework lies in their fundamental approach to manipulation control. Tac-Man implements a two-stage **reactive** paradigm: an execution stage that performs the primary manipulation, followed by a separate recovery stage that corrects contact deviations after they occur. In contrast, TacMan-Turbo integrates these functions into a unified **proactive** process that anticipates and preemptively addresses potential deviations, enabling more fluid and continuous manipulation.

To ensure a fair and rigorous comparison, both methods operate under identical initialization conditions as specified in Section 4.1, including consistent robot configuration, initial grasp state, and interaction direction. This standardized experimental protocol effectively isolates the impact of their differing control strategies, ensuring that performance differences directly reflect the fundamental distinction between reactive and proactive approaches to manipulation.

4.3. Evaluation Metrics

To assess manipulation performance, we employ four complementary metrics that capture both effectiveness and efficiency dimensions. These metrics work together to provide a multifaceted evaluation of the manipulation task.

Success rate. As our primary measure of manipulation effectiveness, success rate employs clear binary criteria tailored to each object type. For articulated objects with standard joints, success requires either rotating a revolute joint beyond 60.0° or extending a prismatic joint beyond 250.0 mm. For the Bézier curve trajectories, success is achieved when the gripper successfully guides the toy train from one end of the track to the other. Manipulations failing to meet these thresholds are classified as unsuccessful, regardless of progress made.

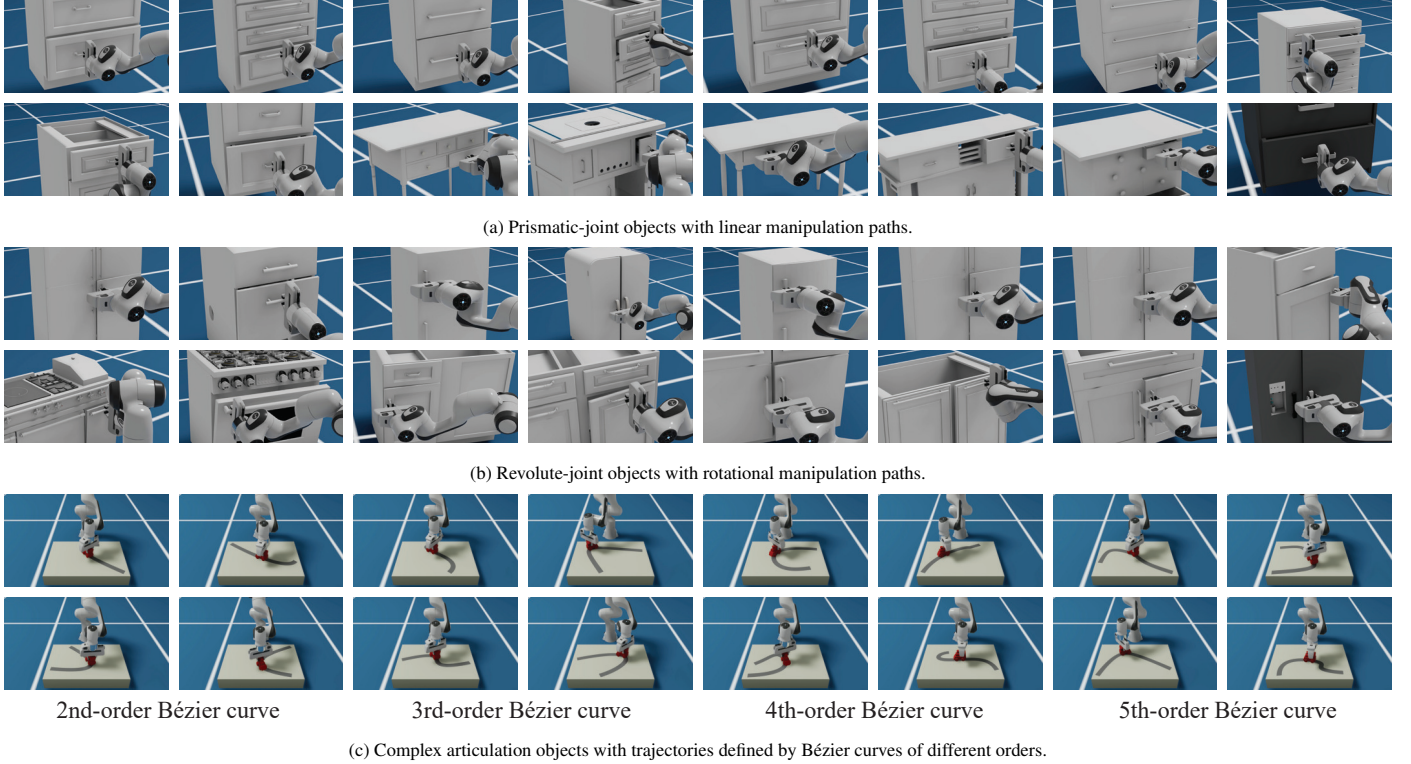


Figure 3: **Simulation test environment and object categories.** Our comprehensive evaluation framework encompasses three progressively complex articulated object categories: (a) 50 prismatic-joint objects featuring linear motion paths, representing the most kinematically straightforward mechanisms; (b) 50 revolute-joint objects with circular motion paths, introducing rotational complexity; and (c) 100 complex articulated objects with trajectories derived from Bézier curves of orders 2–5, simulating sophisticated real-world mechanisms with variable curvature. This systematically designed test suite enables rigorous performance assessment across a spectrum of kinematic complexity. Each case is standardized using initial robot configurations, ensuring fair comparison across manipulation strategies.

Time efficiency. Time efficiency quantifies the temporal performance of successful manipulations, measuring the total duration from task initiation to completion. This metric holds particular significance in applications involving human-robot interaction, where swift task execution directly impacts system practicality and user experience.

Action efficiency. Action efficiency evaluates how directly each motion contributes to task progress, providing insights into the manipulation strategy’s precision and economy of movement. We implement joint-specific calculations: for revolute joints, we compute normalized angular displacement relative to a 60° threshold; for prismatic joints, we measure normalized linear displacement relative to a 250 mm threshold.

For the more complex Bézier curve trajectories, efficiency is determined by progression along the curve’s parameterization $s \in [0, 1]$, where the curve position is defined by:

$$B(s) = \sum_{i=0}^n b_i \binom{n}{i} s^i (1-s)^{n-i}, \quad (28)$$

where b_i represent the control points shaping the curve, $\binom{n}{i}$ is the binomial coefficient, and n indicates the curve order. This unified parameterization enables consistent efficiency measurement across trajectories of varying complexity.

Smoothness of robot joint trajectories. Joint trajectory smoothness serves as both an efficiency indicator and a critical operational metric in robotic manipulation. Smoother trajectories offer multiple benefits: they reflect more efficient motion control, reduce mechanical stress and wear (extending robot lifespan), enhance control precision by limiting vibrations, and improve operational safety by minimizing abrupt movements—particularly important in human-robot interaction scenarios [38].

To quantify smoothness while avoiding the pitfall of artificially smooth but excessively slow trajectories, we employ a time-weighted joint angle jerk. This metric measures the rate of change in joint angle acceleration scaled by task completion time, providing a balanced assessment that accounts for both smoothness and time efficiency.

Together, these four metrics provide a holistic performance profile, capturing the critical dimensions of manipulation capability from both effectiveness and efficiency perspectives.

4.4. Simulation Results

We begin by presenting qualitative results of TacMan-Turbo’s performance in manipulating articulated objects. Using representative examples from each category described in Section 4.1, Fig. 4 illustrates how the predicted handle poses effectively guide the gripper during manipulation tasks. Our observations reveal that when object motion exhibits smooth

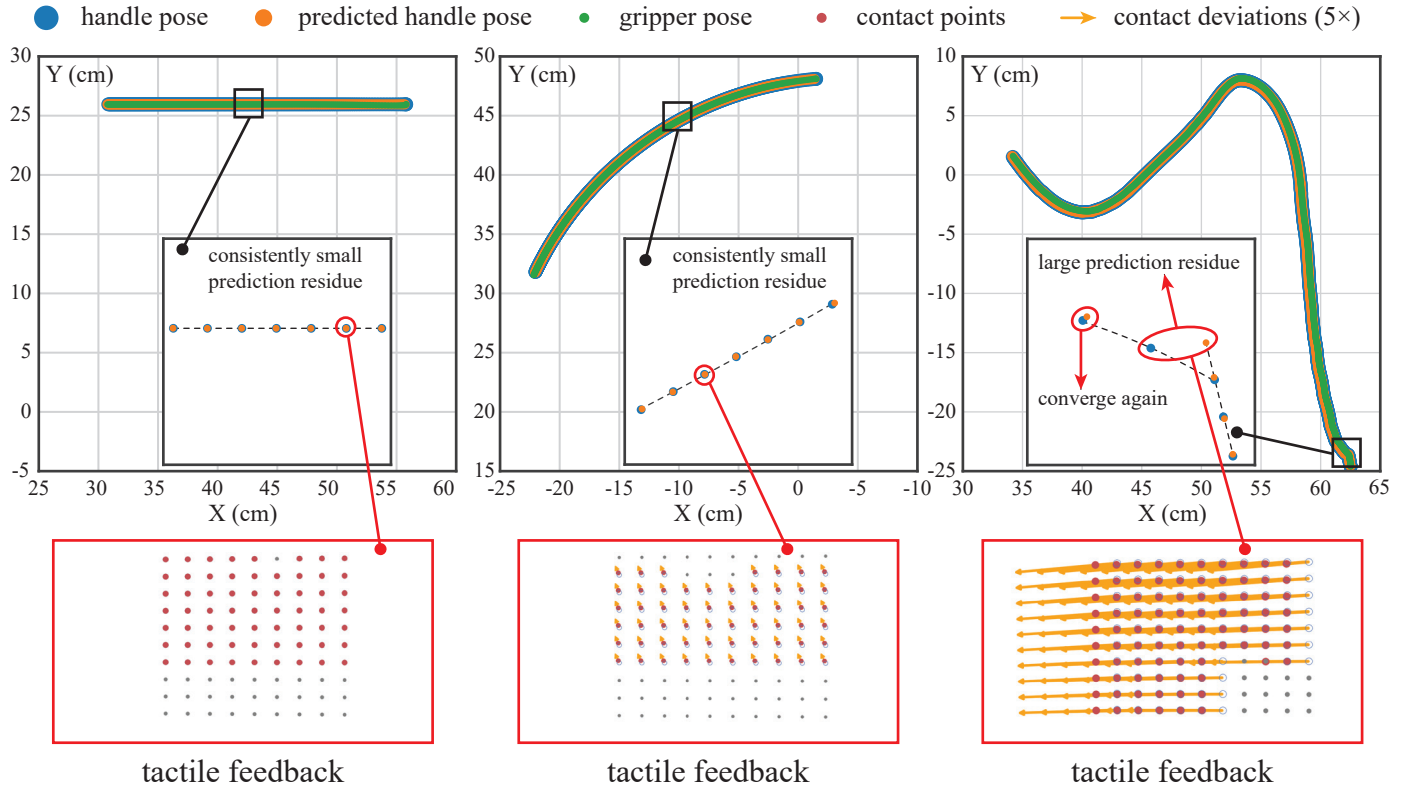


Figure 4: **Qualitative results of simulation studies.** This visualization demonstrates TacMan-Turbo’s performance across three representative cases from our object categories: prismatic (left), revolute (middle), and complex articulation (right). The top row displays trajectory tracking performance with actual handle positions (blue), predicted handle positions (orange), gripper positions (green), and contact points (red), while the bottom row shows corresponding tactile feedback patterns. For objects with consistent kinematic patterns (prismatic and revolute), TacMan-Turbo’s prediction mechanism generates remarkably accurate estimates with minimal residual error, enabling precise trajectory alignment. When confronting complex articulations with sudden directional changes (right column), prediction accuracy temporarily decreases at inflection points, but the system rapidly converges back to the optimal path through iterative correction. The magnified insets highlight these prediction characteristics, demonstrating how TacMan-Turbo maintains effective manipulation even when faced with kinematically challenging scenarios. Contact deviation vectors (orange arrows, magnified 5 \times for visibility) further illustrate how the system continuously adjusts to maintain optimal contact.

and consistent trends, the prediction model captures this behavior with high accuracy. However, as shown in the rightmost column of Fig. 4, abrupt changes in object motion can occasionally introduce prediction errors, stemming from the non-causal nature of our prediction model. Nevertheless, the system demonstrates robust performance through its iterative prediction process, which continually incorporates new observations to correct these errors. These results highlight TacMan-Turbo’s practical effectiveness in handling complex manipulation scenarios commonly encountered in real-world applications. Additional qualitative results are available in the [Supplementary Video S1](#).

Our quantitative analysis evaluates TacMan-Turbo against TacMan using the four metrics defined in Section 4.3.

Success rate results. Both methods achieve perfect 100% manipulation success rates across all 200 test objects spanning 6 categories, as shown in Table 1. This consistent performance demonstrates the fundamental effectiveness of tactile-informed approaches for articulated object manipulation. For comprehensive comparisons between tactile-informed approaches and other manipulation strategies, we refer readers to the detailed analysis in Zhao *et al.* [73].

Table 1: **Success rate (%) comparing TacMan and TacMan-Turbo across articulated object categories.** Both methods achieve perfect manipulation success across all tested joint types, from simple mechanical joints to complex Bézier curves (BC- n) of increasing order.

Joint type	Pri.	Rev.	BC-2	BC-3	BC-4	BC-5
TacMan	100	100	100	100	100	100
TacMan-Turbo	100	100	100	100	100	100

Time efficiency results. While maintaining identical success rates, TacMan-Turbo delivers dramatic improvements in execution speed, as detailed in Fig. 5. Average task completion times for TacMan-Turbo remain consistently around 10 s across all six object categories, compared to TacMan’s typical requirement of over 100 s. Statistical analysis across all 200 test objects confirms this substantial difference between TacMan-Turbo ($M = 7.6$ s, $SD = 2.3$ s) and TacMan ($M = 250.7$ s, $SD = 194.4$ s), $t(199) = 17.7$, $p = 2.1 \times 10^{-52}$.

Action efficiency results. The architectural differences between the two methods are most evident in their action efficiency profiles. As illustrated in Fig. 6a, TacMan’s reactive approach requires dedicated recovery periods that, while necessary for cor-

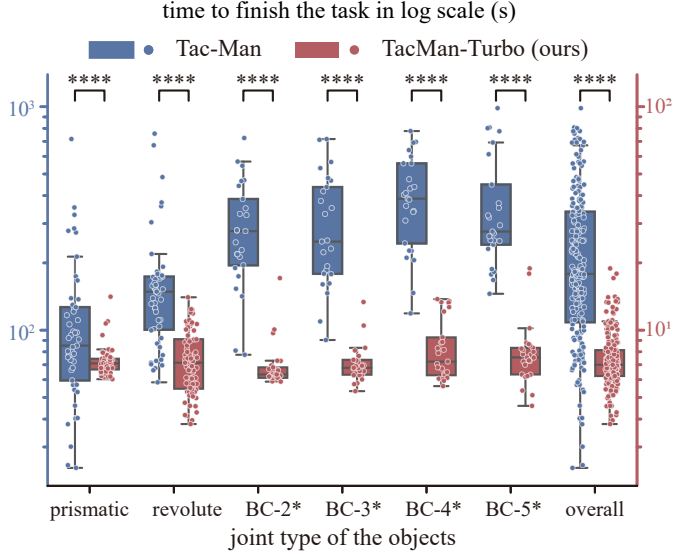
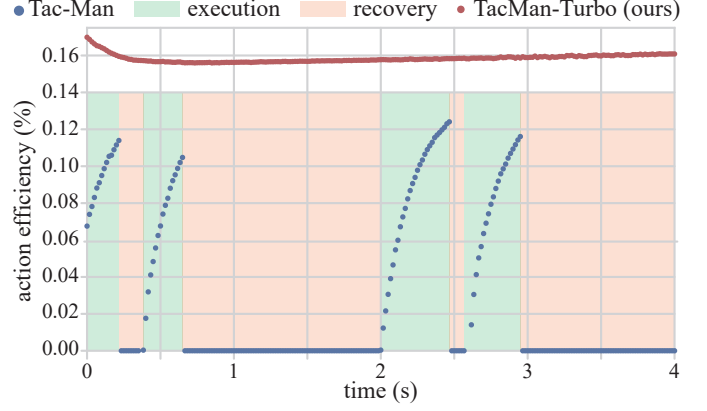


Figure 5: **Time efficiency comparison (logarithmic scale, seconds).** Evaluation of task completion times reveals TacMan-Turbo’s superior efficiency compared to Tac-Man across all tested articulation types. Our method consistently completes manipulation tasks in significantly less time, with performance advantages particularly pronounced for complex articulations. Statistical analysis confirms these improvements are highly significant ($****p < 0.0001$) throughout all joint categories. Box plots display time distributions with medians (center lines), interquartile ranges (boxes), and distribution extent (whiskers at $1.5 \times \text{IQR}$). BC-n denotes Bézier curves of order n.

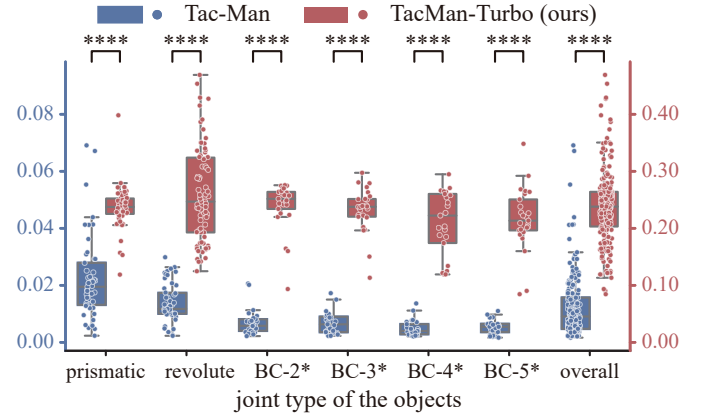
recting contact deviations, do not directly advance the manipulation task. In contrast, TacMan-Turbo’s proactive approach ensures that virtually all actions contribute directly to task progression, eliminating these non-productive recovery phases.

Our quantitative analysis examines both mean efficiency and the Relative Standard Deviation (RSD)—the ratio of standard deviation to mean—across all trials. Results presented in Figs. 6b and 6c demonstrate TacMan-Turbo’s consistently higher average efficiency with minimal variation, even when handling complex Bézier curve trajectories. Statistical analysis across all 200 test objects confirms significant improvements in average action efficiency between TacMan-Turbo ($M = 0.239 \%$, $SD = 0.063 \%$) and Tac-Man ($M = 0.012 \%$, $SD = 0.011 \%$), $t(199) = 52.63$, $p = 8.9 \times 10^{-133}$. Additionally, efficiency stability shows marked improvement, with TacMan-Turbo ($M = 1.0$, $SD = 1.0$) demonstrating significantly lower fluctuation than Tac-Man ($M = 8.8$, $SD = 6.9$), $t(199) = 15.9$, $p = 7.0 \times 10^{-38}$.

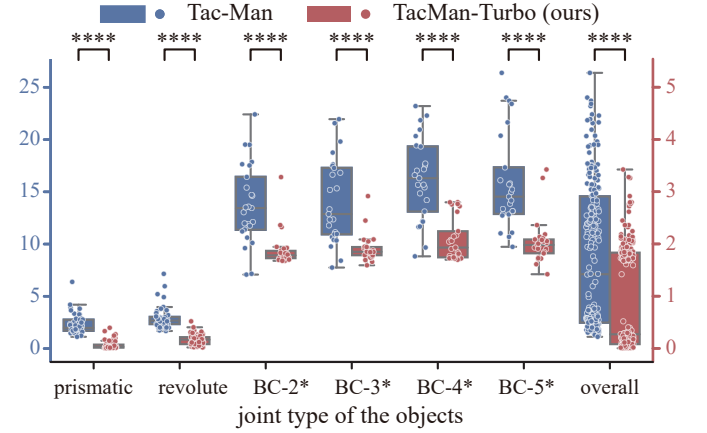
Smoothness results. Trajectory smoothness analysis reveals fundamental behavioral differences between the two approaches. As shown in Fig. 7a, TacMan-Turbo demonstrates more consistent and significantly lower jerk variations compared to Tac-Man. This improvement stems directly from TacMan-Turbo’s proactive strategy, which eliminates the frequent transitions between execution and recovery stages characteristic of Tac-Man. In the reactive approach, compensatory actions to address contact deviations typically require abrupt accelerations and decelerations, resulting in higher jerk mea-



(a) Temporal analysis of action efficiency during manipulation.



(b) Mean action efficiency (%) across object categories.



(c) Relative standard deviation of action efficiency.

Figure 6: **Analysis of action efficiency across manipulation strategies.** Comprehensive evaluation reveals TacMan-Turbo’s superior motion efficiency through three complementary measures. Temporal profiles highlight TacMan-Turbo’s continuous productive motion vs. Tac-Man’s alternating execution-recovery cycles. Mean efficiency measurements confirm TacMan-Turbo’s consistently higher percentage of productive motion across all object categories. Relative standard deviation analysis demonstrates TacMan-Turbo’s more stable and predictable performance. Statistical tests across 200 objects spanning six joint categories show highly significant improvements ($**** p < 0.0001$) in both efficiency magnitude and consistency. BC-n represents Bézier curves of order n; box plots follow conventions established in Fig. 5.

surements.

Comprehensive testing across all 200 objects, summa-

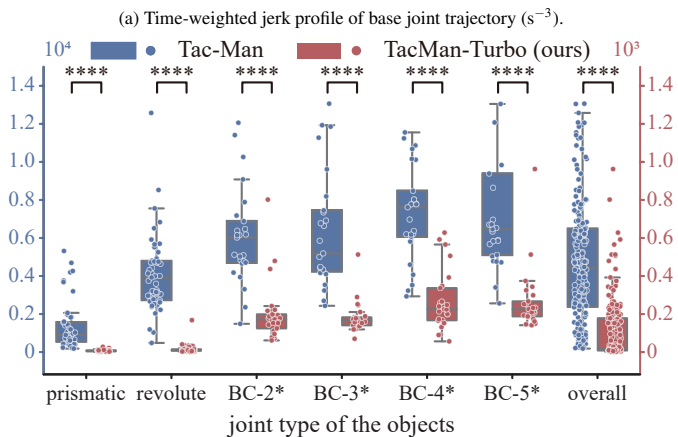
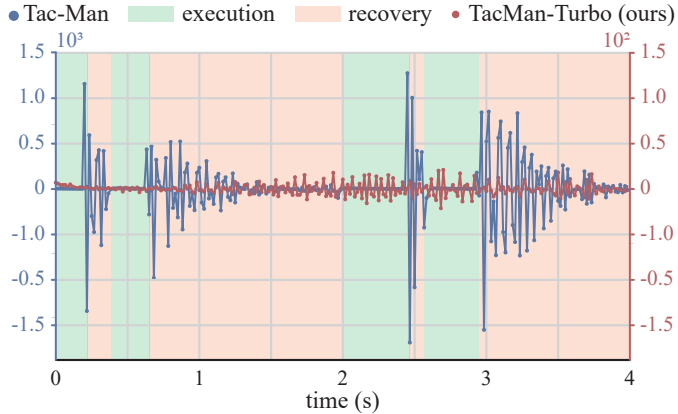


Figure 7: **Analysis of motion smoothness through jerk characteristics.** Motion smoothness evaluation reveals TacMan-Turbo maintains consistently lower jerk magnitudes by eliminating the disruptive transition phases inherent to Tac-Man’s approach. The temporal comparison shows TacMan-Turbo’s continuous motion profile contrasted with Tac-Man’s oscillatory pattern. Statistical analysis across 200 test objects confirms TacMan-Turbo achieves dramatic smoothness gains with standard joint types (prismatic and revolute), while improvements become more moderate with complex Bézier trajectories where challenging pose predictions occasionally necessitate corrective motions. Nevertheless, significant overall improvement (**** $p < 0.0001$) in motion quality is observed across all categories. *Note:* BC- n denotes Bézier curves of order n ; box plots follow conventions established in Fig. 5.

Figure 7b, reveals varying degrees of improvement across object categories. TacMan-Turbo shows the most dramatic smoothness gains with standard prismatic and revolute-joint objects, with more moderate improvements for Bézier-curve trajectories. This performance variation correlates with motion predictability—standard joint types follow consistent patterns that facilitate accurate prediction, while Bézier curves present more variable motion patterns that occasionally lead to mismatches between predicted and actual handle poses. Nevertheless, overall smoothness analysis confirms statistically significant improvement between TacMan-Turbo ($M = 109.82 \text{ s}^{-3}$, $SD = 147.71 \text{ s}^{-3}$) and Tac-Man ($M = 4921.44 \text{ s}^{-3}$, $SD = 3722.49 \text{ s}^{-3}$), $t(199) = 18.27$, $p = 9.11 \times 10^{-45}$.

5. Real-World Experiments

While simulation studies establish TacMan-Turbo’s theoretical advantages, real-world deployment introduces critical challenges absent in simulation: sensor noise, execution uncertainty, and physical constraints. These factors can significantly impact control performance, necessitating comprehensive physical validation. This section presents our real-world experimental evaluation in four complementary parts: experimental setup (Section 5.1), testing protocols (Section 5.2), performance analysis (Section 5.3), and validation on everyday objects (Section 5.4)—including categories not represented in standard articulated object datasets.

5.1. Real-World Experimental Setup

Our physical validation framework integrates three essential components designed to evaluate TacMan-Turbo’s performance under realistic conditions: a robotic manipulation platform, high-fidelity tactile sensing, and diverse test objects with varied kinematic properties.

Robot system setup. Manipulating articulated objects with varied handle paths requires full 6-DoF movement capability in Cartesian space. Our platform employs a 7-DoF Kinova Gen3 robotic arm paired with a Robotiq 2F-85 gripper, providing the necessary workspace coverage and manipulation flexibility. To enable precise contact sensing—crucial for our tactile-based approach—we modified the gripper by replacing its standard pads with two GelSight-type sensors. This integrated system, illustrated in Fig. 8, combines motion versatility with tactile feedback. Overall, the tactile sensor updates contact information at 120 Hz, while the offset velocity is computed at 50 Hz and transmitted to Kinova’s low-level controller, which operates at 1000 Hz.

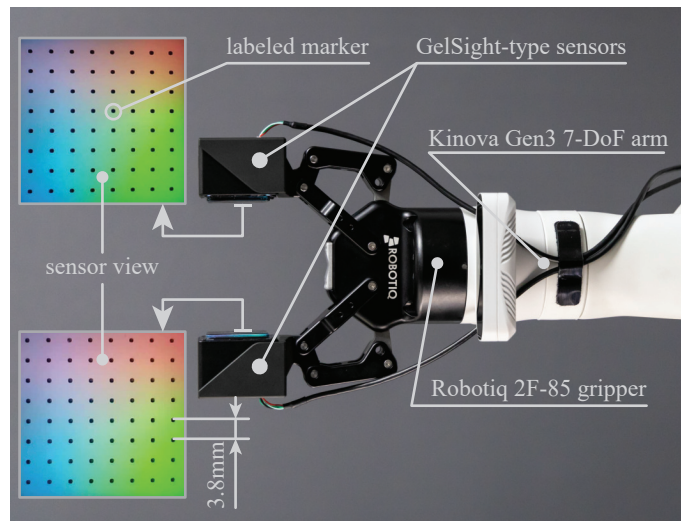


Figure 8: **Physical experimental setup.** The experimental platform consists of a Kinova Gen3 7-DoF robotic arm equipped with a Robotiq 2F-85 parallel gripper. Each gripper finger incorporates a GelSight-type tactile sensor featuring an 8×8 marker grid for precise contact force measurement and deformation tracking.

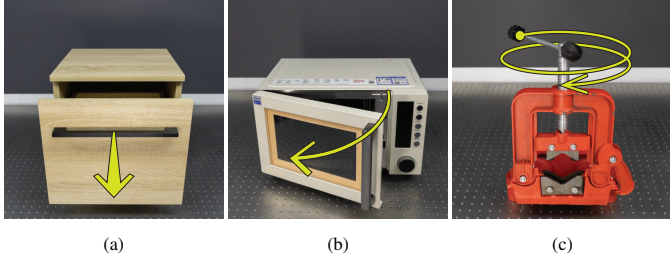


Figure 9: **Test objects for real-world experiments.** The experimental validation employs three articulated objects with distinct kinematic characteristics: (a) a wooden drawer representing pure prismatic joint motion along a linear path, (b) a microwave oven featuring revolute joint dynamics through its door hinge mechanism, and (c) a bench vise with a hand crank generating complex helical motion. These objects collectively challenge the manipulation system across fundamental mechanical joint categories, from simple linear translation to complex compound movements requiring sophisticated trajectory prediction.

Tactile sensors. Accurate contact information between the object and robot is essential for TacMan-Turbo’s operation. Our implementation utilizes two GelSight-type tactile sensors [67], each featuring an 8×8 grid of black markers (Fig. 8). These markers enable precise computation of the relative transformation matrix between gripper and handle through point correspondence matching, as formalized in Eq. (9).

To validate the sensing system’s reliability, we conducted controlled perturbation tests with in-hand objects (Fig. 10). The computed transformations consistently aligned with applied perturbation directions, confirming the system’s ability to accurately estimate relative pose changes—a capability fundamental to the prediction framework described in Section 3.3.

The identification of contact points requires careful parameter calibration to ensure accurate selection within the contact region (Eq. (2)). In our implementation, we dynamically adjust the contact threshold ϵ in Eq. (2) during each trial to the smallest value that yields exactly 9 contact points in the initial contact set \mathcal{C}_i . This adjustment satisfies the mathematical constraints specified in Eqs. (11) and (12) given a maximum of 8 markers along any single line in our setting, ensuring robust contact deviation computation.

Test articulated objects. Following our simulation methodology, we evaluate TacMan-Turbo across three kinematically distinct categories: a drawer with prismatic joints (Fig. 9a), a microwave oven with revolute joints (Fig. 9b), and a vise featuring a helical handle path (Fig. 9c). This selection enables systematic assessment across fundamental joint types while incorporating real-world mechanical complexities such as friction variations and mechanical play.

5.2. Real-World Experiment Protocol

A fair comparison between manipulation approaches requires standardized testing conditions that isolate algorithmic differences from experimental variations. We implemented a rigorous protocol for evaluating TacMan-Turbo against TacMan across all real-world scenarios.

Each experimental trial began with identical initialization conditions: manually established stable grasps on object han-

dles (illustrated in the left column of Fig. 11), ensuring consistent starting contact states. We maintained controlled experimental parameters by testing both methods on the same physical objects with identical initial interaction directions, eliminating potential confounding variables. For the grasping force, since a larger force ensures the non-slipping assumption, we used the lesser of two values: the gripper’s maximum force or the tactile sensor’s force tolerance. In the case of the selected Robotiq 2F-85 gripper, its maximum force is significantly lower than the tactile sensor’s capacity. Therefore, we consistently applied the gripper’s maximum force.

Throughout each manipulation sequence, we recorded two complementary performance metrics: task completion time (measuring overall efficiency) and complete gripper trajectories (capturing motion quality). This dual measurement approach allows a comprehensive assessment of both the temporal efficiency and spatial characteristics of each manipulation strategy.

5.3. Real-World Experiment Results

Our experimental results, presented in Fig. 11, provide comprehensive evidence of both methods’ manipulation capabilities while revealing significant performance distinctions between their approaches.

Manipulation effectiveness. Both TacMan-Turbo and TacMan successfully manipulated all test objects shown in Fig. 9, confirming the fundamental effectiveness of tactile-based strategies for articulated object manipulation. Each method maintained stable contact throughout the manipulation process and completed all assigned tasks. The resulting motion trajectories (middle-right column, Fig. 11) closely followed expected kinematic patterns: linear motion for the prismatic-joint drawer, circular arcs for the revolute-joint microwave door, and extended helical paths for the vise handle. Minor deviations primarily stemmed from manufacturing tolerances inherent in real-world objects.

Performance differences. Despite similar success rates, time efficiency analysis revealed dramatic performance differences between the two approaches. As captured in the middle-left column of Fig. 11, TacMan-Turbo completed manipulation tasks substantially faster, while TacMan had barely initiated object movement at the same point in time. This efficiency gap stemmed from fundamental differences in operational strategies evident in detailed trajectory analysis (right column, Fig. 11).

The operational differences were most pronounced in objects requiring frequent directional adjustments. For the drawer’s linear motion, where the initial interaction direction naturally aligned with the object’s inherent trajectory, both methods demonstrated comparable path following. However, for revolute and helical motions requiring continuous directional adaptation, the methods exhibited markedly different behaviors:

TacMan employed a stepwise exploratory approach, advancing until a predefined threshold was reached. During this process, motion direction gradually drifted from the optimal trajectory, resulting in reduced action efficiency. While this drift was eventually corrected during recovery phases, the

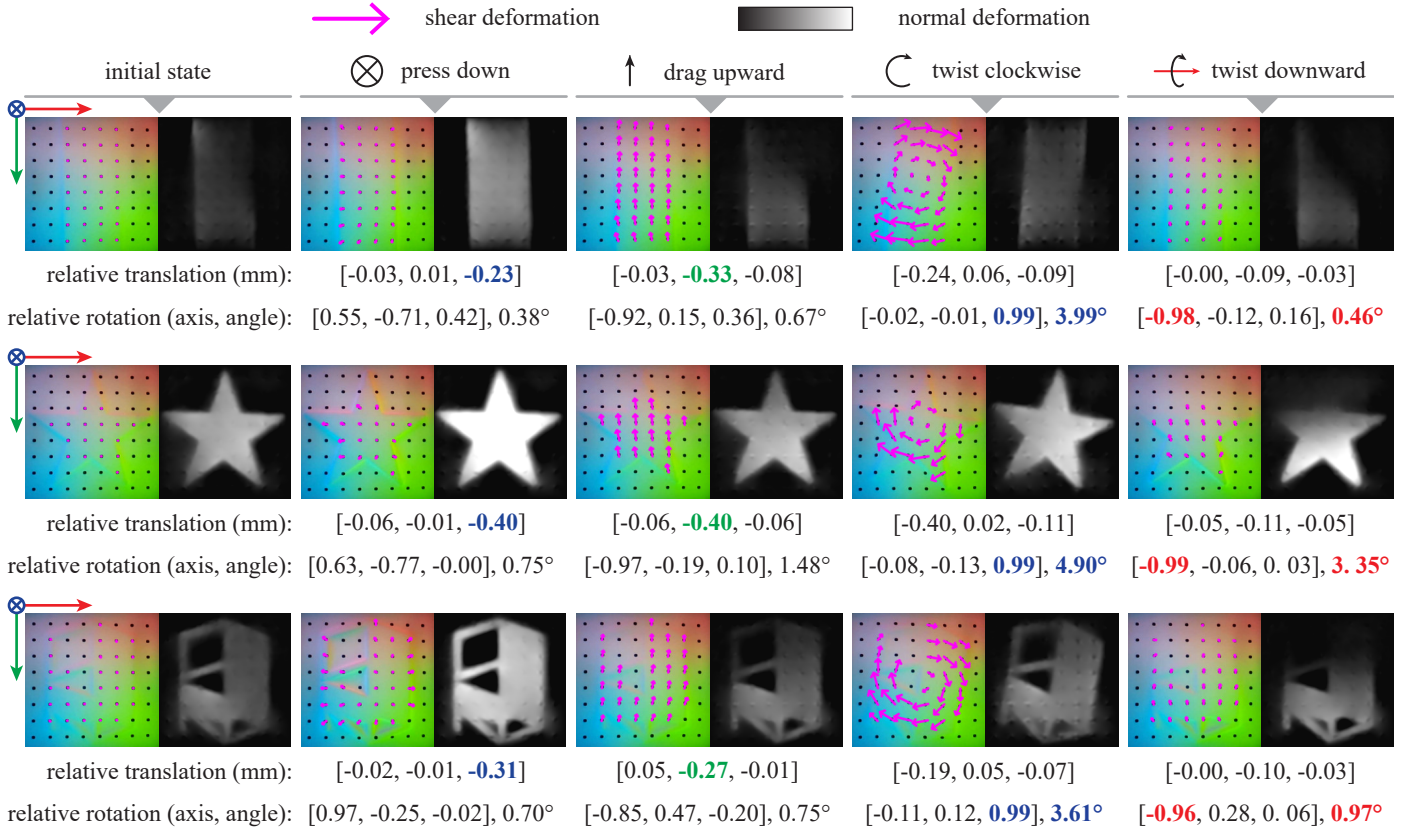


Figure 10: **Tactile-informed pose estimation of in-hand objects.** Precise tracking of object movements during manipulation is demonstrated through tactile feedback across three different objects subjected to five distinct manipulations: initial state, pressing down, dragging upward, and two types of twisting motions. Contact points (marked with purple dots) are tracked to compute relative pose transformations using Eq. (9). The colored grids display marker displacement patterns while grayscale images reveal normal force distribution. Quantitative relative translations (mm) and rotations (axis-angle representation) below each image pair confirm accurate capture of subtle pose changes. Visualization arrows (scaled 7 \times for clarity) illustrate movement direction and magnitude, showing consistent correspondence between applied manipulations and detected transformations across varied object geometries.

repeated cycles of exploration and correction produced non-smooth, zig-zag motion patterns with frequent velocity reversals.

In contrast, TacMan-Turbo leveraged predictive modeling to proactively adjust its motion direction. This continuous adaptation achieved consistently high action efficiency, smoother trajectories, and significantly faster task completion by eliminating the need for separate recovery phases.

These differences in execution time, action efficiency, and trajectory smoothness highlight TacMan-Turbo’s superior performance, successfully translating its theoretical advantages from simulation to real-world application. The results demonstrate TacMan-Turbo’s robustness in practical scenarios, effectively addressing challenges including sensor noise, execution uncertainty, and physical constraints. For detailed visualization of the manipulation process, including tactile sensor feedback throughout execution, we direct readers to the [Supplementary Video S2](#) and [Supplementary Video S3](#).

5.4. Additional Tests on Everyday Objects

To assess TacMan-Turbo’s generalization capabilities beyond laboratory test objects, we extended our evaluation to

include diverse household items encountered in daily environments. These objects, all amenable to secure manipulation using a parallel gripper, present varied kinematic structures and functional challenges not represented in standard datasets.

A battery charging dock (Fig. 12a) exemplifies objects with linear motion paths, where precise trajectory following is essential for secure device removal and to prevent potential damage. A power switch (Fig. 12b) represents safety-critical mechanisms with discrete state transitions, requiring reliable manipulation despite high resistance forces. A coffee maker (Fig. 12c) involves rotational motion, demanding adaptive handling to ensure smooth operation. Lastly, a sewing machine (Fig. 12d) introduces intricate motion patterns with varying resistance caused by its mechanical linkages and operational states.

These objects are not fully represented in standard articulated object datasets, highlighting TacMan-Turbo’s ability to generalize to novel, real-world mechanisms. Starting from stable initial grasps, TacMan-Turbo enabled the robot to successfully execute practical tasks: safely removing devices from charging docks, reliably operating emergency power switches, preparing coffee makers for use, and manipulating sewing machines for basic textile operations.

The consistent success across this diverse set of previously

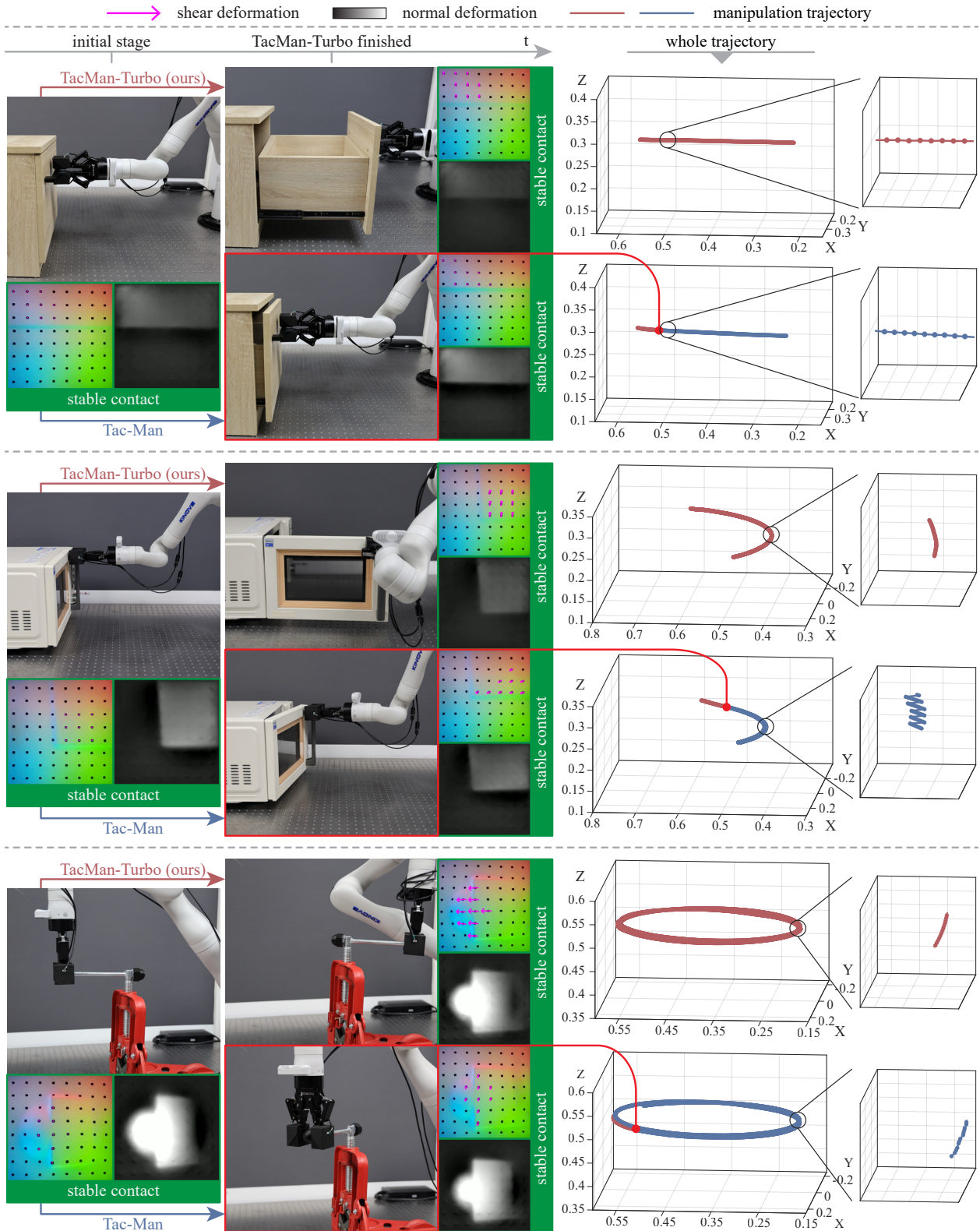


Figure 11: **Real-world experiment results.** Comparative analysis across three articulated objects (drawer, microwave, vise) demonstrates successful manipulation by both methods with clear performance differences. Each row presents a complete manipulation sequence showing initial stable contact (left), manipulation stages (middle), and corresponding 3D trajectories (right). Tactile feedback visualizations display contact force distributions through marker displacement patterns (colored grids) and normal force intensity (grayscale images). While both approaches successfully complete all tasks, TacMan-Turbo consistently delivers more direct trajectories with fewer corrective movements, resulting in reduced completion time, higher action efficiency, and smoother motion profiles. The trajectory plots particularly highlight TacMan-Turbo's more continuous paths (red) vs. Tac-Man's characteristic stop-and-go patterns (blue)

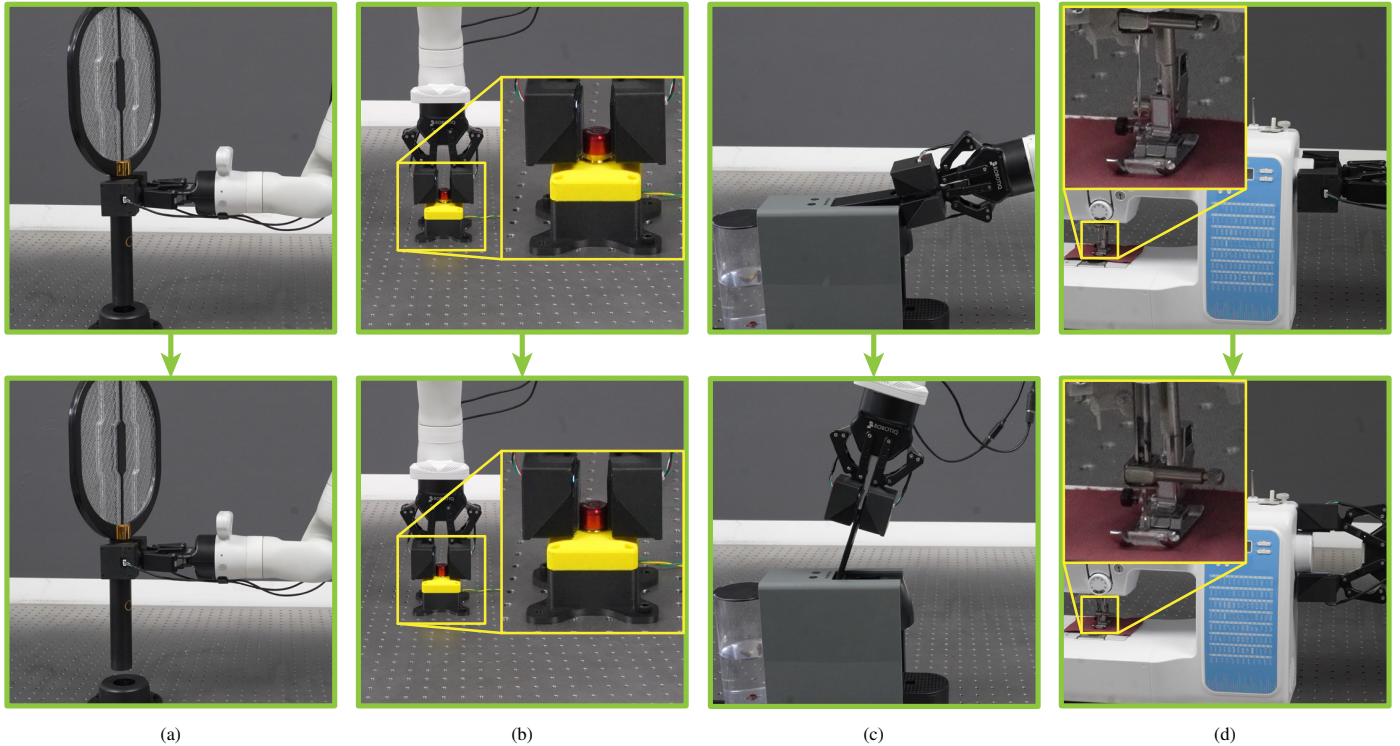


Figure 12: **Tests on various common household objects.** Our TacMan-Turbo approach successfully generalizes to diverse everyday objects without requiring additional tuning. The system effectively manipulates: (a) a battery charging dock requiring precise device extraction, (b) a power switch with discrete on/off state transitions, (c) a coffee maker with rotational lid mechanism, and (d) a sewing machine featuring complex mechanical linkages. Before (top) and after (bottom) images demonstrate successful manipulation for each object. These tests validate TacMan-Turbo’s ability to adapt to varied kinematic constraints and interaction requirements found in common household items, confirming its practical applicability beyond the primary test objects.

unseen objects demonstrates TacMan-Turbo’s robustness and effectiveness in real-world applications. Its ability to handle varying physical properties, motion patterns, and functional requirements underscores its practical utility for everyday manipulation tasks. For detailed visualization of the manipulation process, including tactile sensor feedback throughout execution, we direct readers to the [Supplementary Video S4](#).

6. Discussions

6.1. Comparison with Tac-Man

Both TacMan-Turbo and Tac-Man leverage robot-object contact as the state representation. This approach ensures robustness without requiring pre-defined object kinematics for articulated object manipulation. The effectiveness of this strategy is comprehensively demonstrated through simulation results (Table 1) and validated in real-world experiments (Fig. 11).

In the tactile control context, this modeling framework facilitates direct generation of robot Cartesian motions, eliminating the need for parameter tuning such as PID gain selection. Furthermore, unlike other approaches that also directly generate robot Cartesian motions, this framework avoids reliance on manually-defined tactile features. Instead, it leverages contact points for frame registration, making it inherently robust and agnostic to variations in handle shapes and structures.

Although both approaches share a similar state representation, they address the manipulation problem fundamentally differently. Tac-Man adopts a **reactive** strategy, prioritizing compensation for the current contact deviation—denoted as the deviation at step i . This approach temporarily halts object manipulation and focuses exclusively on deviation correction. Consequently, the process naturally divides into two distinct stages: execution and recovery, as evident in Fig. 6a and the zig-zag trajectories observed in Fig. 11. While this formulation enhances robustness by ensuring timely compensation, it introduces inefficiencies, as the recovery stage does not directly advance the manipulation task. Additionally, transitions between execution and recovery stages produce non-smooth trajectories, as highlighted in Fig. 7a and Fig. 11. Although Tac-Man incorporates multi-step exploration in real deployments to mitigate these limitations, the fundamental drawbacks of the reactive formulation remain.

In contrast, TacMan-Turbo’s core motivation explores whether robust manipulation can be achieved without interrupting the object interaction process. This question drives the development of TacMan-Turbo’s **proactive** formulation. Unlike reactive approaches, this formulation must account not only for the current i -step contact deviation but also anticipate the impact of the future $i + 1$ -step contact deviation caused by continuous, non-halting manipulation, as described in Eq. (5).

This noncausal formulation, which incorporates future state information, introduces challenges that previous approaches—

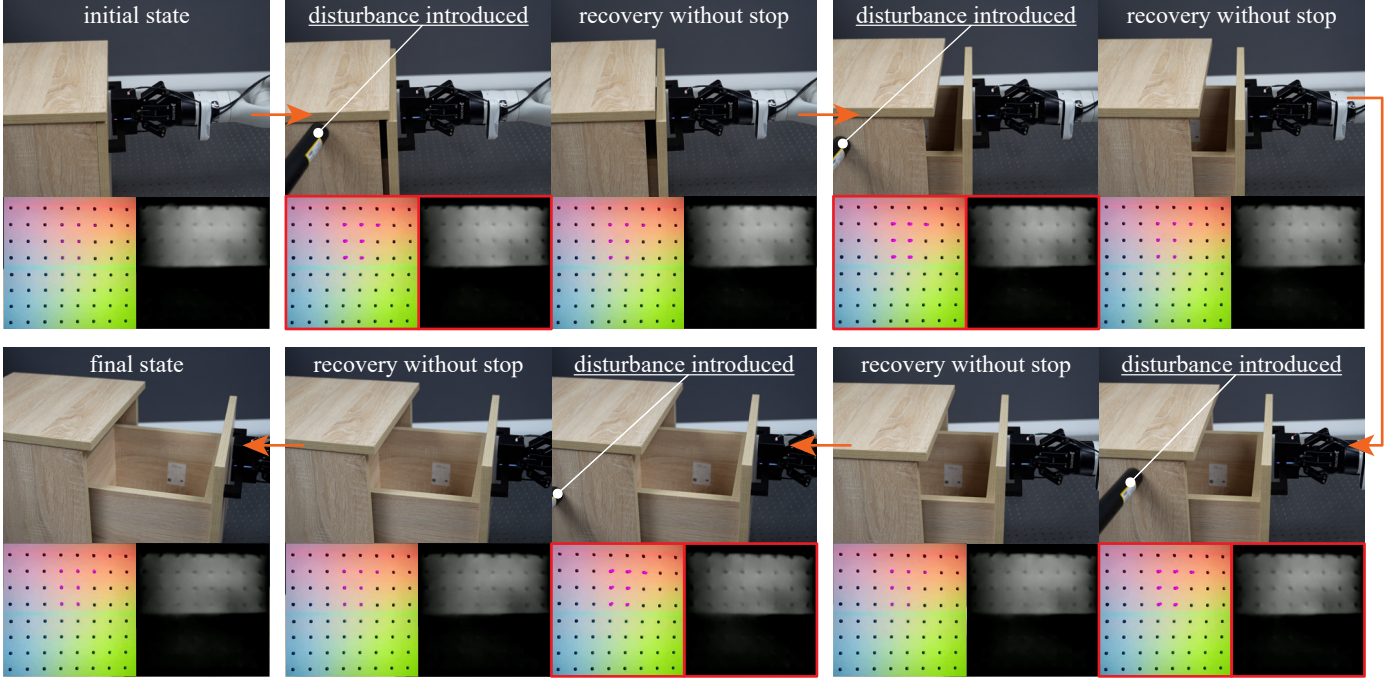


Figure 13: **Manipulation under disturbance.** The efficiency gains enabled by TacMan-Turbo do not compromise its robustness against unexpected disturbances that frequently occur in human-centric environments. Unlike previous reactive paradigms [73] that require stopping for reactive adjustments, TacMan-Turbo can maintain manipulation progress continuously. Detailed manipulation processes are available in the [Supplementary Video S5](#).

where contact deviation served solely as an error signal—cannot address. To overcome this, TacMan-Turbo leverages the local kinematics of the object inherently embedded within contact deviations. By extracting and utilizing this structural information, TacMan-Turbo enables reasonable prediction of future states, effectively solving the noncausal problem.

This proactive formulation streamlines the previous execution-recovery cycle into a seamless and consistent manipulation process. As a result, it delivers significant performance gains, including an order-of-magnitude improvement in time efficiency, consistently high action efficiency, and smooth trajectories free from acceleration-deceleration cycles—all while maintaining manipulation effectiveness. Furthermore, this framework maintains robustness against unexpected disturbances that frequently occur in human-centric environments while continuing the manipulation process without stopping for reactive compensation, as shown in Fig. 13.

6.2. Base Velocity Effects and Acquisition

The performance of TacMan-Turbo depends critically on the initial base velocity $u_0^{g_i}$ introduced in Section 3.2. While our primary experiments utilized manually assigned values for this parameter, understanding both its effects on system performance and methods for its automated acquisition has significant implications for practical deployment. We analyze the magnitude and direction components separately to provide a more structured understanding of their respective influences.

Magnitude effect and acquisition. Velocity magnitude directly impacts manipulation efficiency, with higher values generally

enabling faster task completion. However, two fundamental constraints limit the applicable magnitude: the manipulator’s physical capabilities and the tactile sensors’ characteristics.

The manipulator constraint is straightforward— $u_0^{g_i}$ cannot exceed the maximum permissible end-effector velocity. The tactile sensor constraint presents more nuanced considerations. For accurate contact deviation detection, differences in consecutive sensor readings (induced by $u_0^{g_i}$) must remain below the threshold that would trigger relative slippage between sensor and object. The most limiting scenario occurs when $u_0^{g_i}$ is perpendicular to the optimal interaction direction, as this configuration contributes maximally to contact deviation. Under these conditions, the constraint is formalized as:

$$u_0^{g_i} \leq \gamma f, \quad (29)$$

where γ represents the critical slippage threshold and f denotes sampling frequency. This formulation reveals two pathways to enabling higher base velocities and thus improving manipulation efficiency: increasing surface roughness (which raises γ) or elevating the sampling frequency.

Our implementation employed vision-based tactile sensors limited by their image sensors to approximately 100 Hz sampling frequency. Alternative sensing technologies, such as capacitive or 6D force/torque sensors, can operate at frequencies exceeding 1000 Hz [1], suggesting promising opportunities for substantial efficiency gains through TacMan-Turbo adaptation to these advanced modalities.

Direction effect and acquisition. The direction of base velocity profoundly influences manipulation efficiency. Greater align-

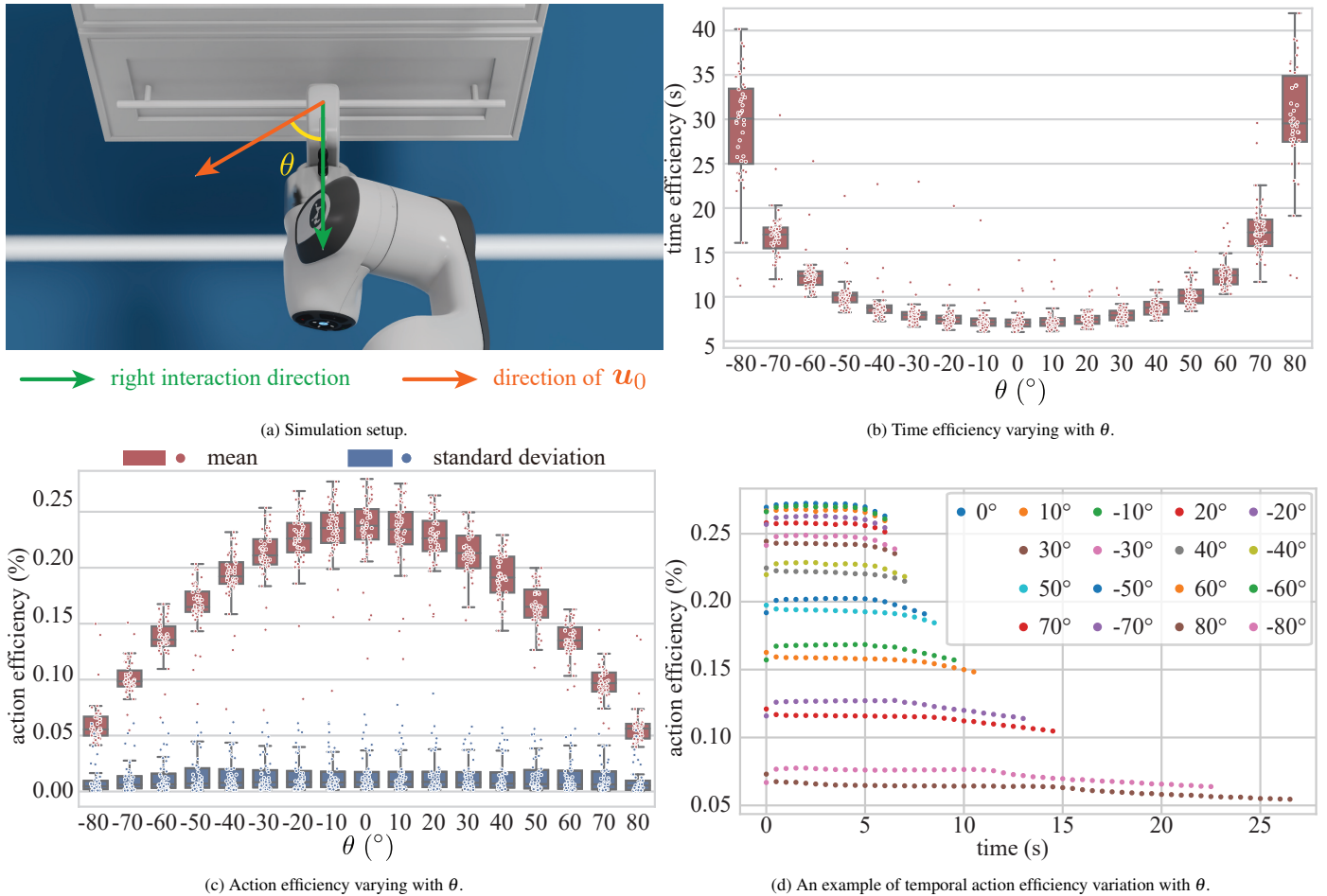


Figure 14: **Effects of base velocity direction.** We investigate how initial directional alignment impacts manipulation performance. (a) The simulation setup measures the angle θ between the correct interaction direction (green arrow) and the initial motion direction u_0^{gi} (orange arrow). (b) Time efficiency results reveal significant performance deterioration as θ increases in magnitude, with optimal performance near $\theta = 0^\circ$. (c) Action efficiency peaks when initial direction closely aligns with the correct interaction direction and gradually decreases with increasing angular deviation. (d) The temporal progression further illustrates how different initial angles affect performance throughout the manipulation process, with properly aligned initial directions maintaining consistently higher efficiency. These findings highlight the critical importance of directional alignment in manipulation tasks.

ment between u_0^{gi} and the object’s optimal interaction direction yields higher first-step action efficiency (as defined in Section 4.1). This initial efficiency advantage propagates through subsequent steps, potentially maintaining elevated performance throughout the entire manipulation process.

To quantify this relationship, we conducted systematic simulations across 50 prismatic-joint objects (Fig. 14a), varying the angle θ between u_0^{gi} and the optimal direction. The results confirm our theoretical expectations: both time efficiency (Fig. 14b) and action efficiency (Fig. 14c) reach maximum values at $\theta = 0$ and deteriorate as θ increases. Furthermore, Fig. 14d reveals that per-step action efficiency maintains remarkable consistency throughout the manipulation process, closely tracking the first-step efficiency and achieving its peak at perfect alignment ($\theta = 0$).

These findings not only validate our theoretical framework but also highlight the critical importance of appropriate base velocity direction selection. They further suggest promising research directions for automating preliminary directional information acquisition. Recent advances in vision-based direction

estimation [31] offer particularly promising pathways. While such methods inevitably introduce some estimation noise, they enhance TacMan-Turbo’s operational autonomy. Moreover, our framework’s inherent robustness could effectively compensate for moderate directional inaccuracies, as demonstrated by the gradual performance degradation shown in Fig. 14b.

7. Conclusion and Future Work

This paper introduces TacMan-Turbo, a novel proactive control framework that successfully resolves the persistent trade-off between efficiency and effectiveness in articulated object manipulation. By fundamentally reframing contact deviations as valuable kinematic information rather than mere error signals, our approach enables proactive control adjustments that significantly enhance manipulation efficiency while maintaining robust performance across diverse articulated mechanisms.

Our comprehensive evaluation—encompassing 200 simulated articulated objects with varied kinematic structures and multiple real-world experiments across fundamental joint

types—demonstrates that TacMan-Turbo achieves perfect manipulation success rates (100%) while delivering substantial improvements in time efficiency, action efficiency, and trajectory smoothness compared to previous approaches. The statistical significance of these performance gains (p-values < 0.0001) confirms that TacMan-Turbo effectively addresses the effectiveness-efficiency trade-off that has challenged existing manipulation methods.

This work represents an important advancement toward practical robot deployment in human-centric environments, where robots must manipulate articulated objects reliably and efficiently without precise pre-provided kinematic models. The ability to extract and leverage kinematic insights directly from tactile feedback enables robots to adapt to uncertain object structures while executing smooth, efficient movements—a capability essential for robots operating effectively in dynamic, everyday settings alongside humans.

Several promising directions for future research emerge from this work. First, developing adaptive methods for base velocity optimization could further enhance efficiency by dynamically adjusting control parameters in response to object characteristics. Second, extending the framework to support diverse tactile sensing modalities would broaden its applicability across robot platforms with different sensing capabilities. Finally, incorporating learning-based approaches for predicting object behavior could enable even more anticipatory control strategies. These enhancements will not only further boost the framework’s efficiency but also facilitate its application in increasingly complex, unstructured real-world environments.

Acknowledgment

Our sincere thanks go to Yuanhong Zeng (UCLA) and Qian Long (UCLA) for their suggestion in driving Kinova, Lei Yan (LeapZenith AI Research) for mechanical design support, Yida Niu (PKU) for demo shooting, and Ms. Hailu Yang (PKU) for her assistance in procuring every piece of raw material necessary for this research. This work is supported in part by the National Science and Technology Major Project (2022ZD0114900), the National Natural Science Foundation of China (62376031), the Beijing Nova Program, the State Key Lab of General AI at Peking University, the PKU-BingJi Joint Laboratory for Artificial Intelligence, and the National Comprehensive Experimental Base for Governance of Intelligent Society, Wuhan East Lake High-Tech Development Zone.

References

- [1] ATI Industrial Automation, ATI Multi-Axis Force/Torque Sensor System, Available online: <https://www.ati-ia.com/products/ft/sensors.aspx>, accessed: 2025, 2025.
- [2] A. D. Berger, P. K. Khosla, Using tactile data for real-time feedback, *International Journal of Robotics Research (IJRR)* 10 (2) (1991) 88–102.
- [3] C. M. Boutry, M. Negre, M. Jorda, O. Vardoulis, A. Chortos, O. Khatib, Z. Bao, A hierarchically patterned, bioinspired e-skin able to detect the direction of applied pressure for robotics, *Science Robotics* 3 (24) (2018) eaa06914.
- [4] S. Brahmabhatt, C. Ham, C. C. Kemp, J. Hays, Contactdb: Analyzing and predicting grasp contact via thermal imaging, in: *Proceedings of Conference on Computer Vision and Pattern Recognition (CVPR)*, 2019.
- [5] F. Burget, A. Hornung, M. Bennewitz, Whole-body motion planning for manipulation of articulated objects, in: *IEEE International Conference on Robotics and Automation (ICRA)*, 2013.
- [6] N. Chen, H. Zhang, R. Rink, Edge tracking using tactile servo, in: *IEEE/RSJ International Conference on Intelligent Robots and Systems (IROS)*, 1995.
- [7] Y. Chen, T. Wu, S. Wang, X. Feng, J. Jiang, Z. Lu, S. McAleer, H. Dong, S.-C. Zhu, Y. Yang, Towards human-level bimanual dexterous manipulation with reinforcement learning, in: *Proceedings of Advances in Neural Information Processing Systems (NeurIPS)*, 2022.
- [8] C.-A. Cheng, M. Mukadam, J. Issac, S. Birchfield, D. Fox, B. Boots, N. Ratliff, Rmpflow: A geometric framework for generation of multitask motion policies, *IEEE Transactions on Automation Science and Engineering (T-ASE)* 18 (3) (2021) 968–987.
- [9] S. Chitta, B. Cohen, M. Likhachev, Planning for autonomous door opening with a mobile manipulator, in: *IEEE International Conference on Robotics and Automation (ICRA)*, 2010.
- [10] T. Dai, J. Wong, Y. Jiang, C. Wang, C. Gokmen, R. Zhang, J. Wu, L. Fei-Fei, ACDC: Automated Creation of Digital Cousins for Robust Policy Learning, in: *Conference on Robot Learning (CoRL)*, 2024.
- [11] A. J. Davison, I. D. Reid, N. D. Molton, O. Stasse, MonoSLAM: Real-time single camera SLAM, *Transactions on Pattern Analysis and Machine Intelligence (TPAMI)* 29 (6) (2007) 1052–1067.
- [12] A. B. Dawood, C. Coppola, K. Althoefer, Learning Decoupled Multi-touch Force Estimation, Localization and Stretch for Soft Capacitive E-skin, in: *IEEE International Conference on Robotics and Automation (ICRA)*, 2023.
- [13] J. A. Fishel, G. E. Loeb, Sensing tactile microvibrations with the Bio-Tac—Comparison with human sensitivity, in: *International Conference on Biomedical Robotics and Biomechanics (BioRob)*, 2012.
- [14] Z. Fu, T. Z. Zhao, C. Finn, Mobile ALOHA: Learning Bimanual Mobile Manipulation with Low-Cost Whole-Body Teleoperation, in: *Conference on Robot Learning (CoRL)*, 2024.
- [15] H. Geng, Z. Li, Y. Geng, J. Chen, H. Dong, H. Wang, Partmanip: Learning cross-category generalizable part manipulation policy from point cloud observations, in: *Proceedings of Conference on Computer Vision and Pattern Recognition (CVPR)*, 2023.
- [16] H. Geng, H. Xu, C. Zhao, C. Xu, L. Yi, S. Huang, H. Wang, Gapartnet: Cross-category domain-generalizable object perception and manipulation via generalizable and actionable parts, in: *Proceedings of Conference on Computer Vision and Pattern Recognition (CVPR)*, 2023.
- [17] R. Gong, J. Huang, Y. Zhao, H. Geng, X. Gao, Q. Wu, W. Ai, Z. Zhou, D. Terzopoulos, S.-C. Zhu, ARNOLD: A Benchmark for Language-Grounded Task Learning With Continuous States in Realistic 3D Scenes, in: *Proceedings of International Conference on Computer Vision (ICCV)*, 2023.
- [18] P. L. Gould, Y. Feng, *Introduction to linear elasticity*, vol. 2, Springer, 1994.
- [19] K. Hausman, S. Niekum, S. Osentoski, G. S. Sukhatme, Active articulation model estimation through interactive perception, in: *IEEE International Conference on Robotics and Automation (ICRA)*, 2015.
- [20] R. Hu, W. Li, O. Van Kaick, A. Shamir, H. Zhang, H. Huang, Learning to predict part mobility from a single static snapshot, *ACM Transactions on Graphics (TOG)* 36 (6) (2017) 1–13.
- [21] W. Kabsch, A solution for the best rotation to relate two sets of vectors, *Acta Crystallographica Section A: Crystal Physics, Diffraction, Theoretical and General Crystallography* 32 (5) (1976) 922–923.
- [22] Z. Kappassov, J.-A. Corrales, V. Perdereau, Touch driven controller and tactile features for physical interactions, *Robotics and Autonomous Systems* 123 (2020) 103332.
- [23] Y. Karayiannidis, C. Smith, F. E. V. Barrientos, P. Ögren, D. Kragic, An adaptive control approach for opening doors and drawers under uncertainties, *IEEE Transactions on Robotics (T-RO)* 32 (1) (2016) 161–175.
- [24] Y. Karayiannidis, C. Smith, F. E. Vina, P. Ögren, D. Kragic, “Open sesame!” adaptive force/velocity control for opening unknown doors, in: *IEEE/RSJ International Conference on Intelligent Robots and Systems (IROS)*, 2012.
- [25] N. F. Lepora, J. Lloyd, Pose-based tactile servoing: Controlled soft touch

- using deep learning, *IEEE Robotics and Automation Magazine (RA-M)* 28 (4) (2021) 43–55.
- [26] Q. Li, C. Schürmann, R. Haschke, H. J. Ritter, A Control Framework for Tactile Servoing., in: *Robotics: Science and Systems (RSS)*, 2013.
- [27] W. Li, M. Wang, J. Li, Y. Su, D. K. Jha, X. Qian, K. Althoefer, H. Liu, L³ F-TOUCH: A Wireless GelSight with Decoupled Tactile and Three-axis Force Sensing, *IEEE Robotics and Automation Letters (RA-L)*.
- [28] W. Li, Z. Zhao, L. Cui, W. Zhang, H. Liu, L.-A. Li, Y. Zhu, MiniTac: An Ultra-Compact 8 mm Vision-Based Tactile Sensor for Enhanced Palpation in Robot-Assisted Minimally Invasive Surgery, *IEEE Robotics and Automation Letters (RA-L)* 9 (12) (2024) 11170–11177.
- [29] X. Li, H. Wang, L. Yi, L. J. Guibas, A. L. Abbott, S. Song, Category-level articulated object pose estimation, in: *Proceedings of Conference on Computer Vision and Pattern Recognition (CVPR)*, 2020.
- [30] Y. Li, W. Du, C. Yu, P. Li, Z. Zhao, T. Liu, C. Jiang, Y. Zhu, S. Huang, Taccel: Scaling Up Vision-based Tactile Robotics via High-performance GPU Simulation, arXiv preprint arXiv:2504.12908.
- [31] Y. Li, W. H. Leng, Y. Fang, B. Eisner, D. Held, FlowBotHD: History-Aware Diffuser Handling Ambiguities in Articulated Objects Manipulation, in: *Conference on Robot Learning (CoRL)*, 2024.
- [32] Y. Li, B. Liu, Y. Geng, P. Li, Y. Yang, Y. Zhu, T. Liu, S. Huang, Grasp multiple objects with one hand, *IEEE Robotics and Automation Letters (RA-L)*.
- [33] L. Liu, W. Xu, H. Fu, S. Qian, Q. Yu, Y. Han, C. Lu, AKB-48: a real-world articulated object knowledge base, in: *Proceedings of Conference on Computer Vision and Pattern Recognition (CVPR)*, 2022.
- [34] Y. Liu, B. Jia, R. Lu, J. Ni, S.-C. Zhu, S. Huang, Building Interactable Replicas of Complex Articulated Objects via Gaussian Splatting, in: *Proceedings of International Conference on Learning Representations (ICLR)*, 2025.
- [35] J. Lloyd, N. F. Lepora, Pose-and-shear-based tactile servoing, *International Journal of Robotics Research (IJRR)* 43 (7) (2024) 1024–1055.
- [36] J. Lv, Q. Yu, L. Shao, W. Liu, W. Xu, C. Lu, Sagec-system: Towards sample-efficient, generalizable, compositional, and incremental robot learning, in: *IEEE International Conference on Robotics and Automation (ICRA)*, 2022.
- [37] K. M. Lynch, F. C. Park, *Modern Robotics*, Cambridge University Press, 2017.
- [38] S. Macfarlane, E. A. Croft, Jerk-bounded manipulator trajectory planning: design for real-time applications, *IEEE Transactions on Robotics and Automation (T-RA)* 19 (1) (2003) 42–52.
- [39] R. Martín-Martín, O. Brock, Coupled recursive estimation for online interactive perception of articulated objects, *International Journal of Robotics Research (IJRR)* 41 (8) (2022) 741–777.
- [40] M. Mittal, D. Hoeller, F. Farshidian, M. Hutter, A. Garg, Articulated object interaction in unknown scenes with whole-body mobile manipulation, in: *IEEE/RSJ International Conference on Intelligent Robots and Systems (IROS)*, 2022.
- [41] K. Mo, S. Zhu, A. X. Chang, L. Yi, S. Tripathi, L. J. Guibas, H. Su, Partnet: A large-scale benchmark for fine-grained and hierarchical part-level 3D object understanding, in: *Proceedings of Conference on Computer Vision and Pattern Recognition (CVPR)*, 2019.
- [42] C. Moses, M. Noseworthy, L. P. Kaelbling, T. Lozano-Pérez, N. Roy, Visual Prediction of Priors for Articulated Object Interaction, in: *IEEE International Conference on Robotics and Automation (ICRA)*, 2020.
- [43] R. Mur-Artal, J. M. M. Montiel, J. D. Tardos, ORB-SLAM: A versatile and accurate monocular SLAM system, *IEEE Transactions on Robotics (T-RO)* 31 (5) (2015) 1147–1163.
- [44] J. Ni, Y. Liu, R. Lu, Z. Zhou, S.-C. Zhu, Y. Chen, S. Huang, Compositional neural scene reconstruction with generative diffusion prior, in: *Proceedings of Conference on Computer Vision and Pattern Recognition (CVPR)*, 2025.
- [45] P. Pastor, H. Hoffmann, T. Asfour, S. Schaal, Learning and generalization of motor skills by learning from demonstration, in: *IEEE International Conference on Robotics and Automation (ICRA)*, 2009.
- [46] Y. Qin, H. Su, X. Wang, From one hand to multiple hands: Imitation learning for dexterous manipulation from single-camera teleoperation, *IEEE Robotics and Automation Letters (RA-L)* 7 (4) (2022) 10873–10881.
- [47] Y. Qin, W. Yang, B. Huang, K. Van Wyk, H. Su, X. Wang, Y.-W. Chao, D. Fox, Anyteleop: A general vision-based dexterous robot arm-hand teleoperation system, in: *Robotics: Science and Systems (RSS)*, 2023.
- [48] C. Schöllner, V. Aravatinos, F. Lay, A. Knoll, What the constant velocity model can teach us about pedestrian motion prediction, *IEEE Robotics and Automation Letters (RA-L)* 5 (2) (2020) 1696–1703.
- [49] Y. She, S. Wang, S. Dong, N. Sunil, A. Rodriguez, E. Adelson, Cable manipulation with a tactile-reactive gripper, *International Journal of Robotics Research (IJRR)* 40 (12-14) (2021) 1385–1401.
- [50] B. Siciliano, O. Khatib, T. Kröger, *Springer handbook of robotics*, vol. 200, Springer, 2008.
- [51] P. Sikka, H. Zhang, S. Sutphen, Tactile servo: Control of touch-driven robot motion, in: *Experimental Robotics III: The 3rd International Symposium*, Kyoto, Japan, October 28–30, 1993, Springer, 219–233, 2005.
- [52] A. Tekden, M. P. Deisenroth, Y. Bekiroglu, Grasp Transfer based on Self-Aligning Implicit Representations of Local Surfaces, *IEEE Robotics and Automation Letters (RA-L)*.
- [53] Y. Urakami, A. Hodgkinson, C. Carlin, R. Leu, L. Rigazio, P. Abbeel, Doorgym: A scalable door opening environment and baseline agent, in: *Proceedings of Advances in Neural Information Processing Systems (NeurIPS)*, 2019.
- [54] W. Wang, Z. Zhao, Z. Jiao, Y. Zhu, S.-C. Zhu, H. Liu, Rearrange indoor scenes for human-robot co-activity, in: *IEEE International Conference on Robotics and Automation (ICRA)*, 2023.
- [55] B. Ward-Cherrier, N. Pestell, L. Cramphorn, B. Winstone, M. E. Giannaccini, J. Rossiter, N. F. Lepora, The tactip family: Soft optical tactile sensors with 3D-printed biomimetic morphologies, *Soft Robotics* 5 (2) (2018) 216–227.
- [56] L. Weiss, A. Sanderson, C. Neuman, Dynamic sensor-based control of robots with visual feedback, *IEEE Journal on Robotics and Automation* 3 (5) (1987) 404–417.
- [57] T. Welschehold, C. Dornhege, W. Burgard, Learning mobile manipulation actions from human demonstrations, in: *IEEE/RSJ International Conference on Intelligent Robots and Systems (IROS)*, 2017.
- [58] A. Wilson, H. Jiang, W. Lian, W. Yuan, Cable routing and assembly using tactile-driven motion primitives, in: *IEEE International Conference on Robotics and Automation (ICRA)*, 2023.
- [59] J. Wong, A. Tung, A. Kurenkov, A. Mandlekar, L. Fei-Fei, S. Savarese, R. Martín-Martín, Error-aware imitation learning from teleoperation data for mobile manipulation, in: *Conference on Robot Learning (CoRL)*, 2022.
- [60] F. Xiang, Y. Qin, K. Mo, Y. Xia, H. Zhu, F. Liu, M. Liu, H. Jiang, Y. Yuan, H. Wang, et al., Sapien: A simulated part-based interactive environment, in: *Proceedings of Conference on Computer Vision and Pattern Recognition (CVPR)*, 2020.
- [61] H. Xiong, Q. Li, Y.-C. Chen, H. Bharadhwaj, S. Sinha, A. Garg, Learning by watching: Physical imitation of manipulation skills from human videos, in: *IEEE/RSJ International Conference on Intelligent Robots and Systems (IROS)*, 2021.
- [62] Z. Xu, Z. He, S. Song, Universal manipulation policy network for articulated objects, *IEEE Robotics and Automation Letters (RA-L)* 7 (2) (2022) 2447–2454.
- [63] Z. Xu, Y. She, LeTac-MPC: Learning Model Predictive Control for Tactile-Reactive Grasping, *IEEE Transactions on Robotics (T-RO)* 40 (2024) 4376–4395.
- [64] Y. Yang, X. Wei, N. Zhang, J. Zheng, X. Chen, Q. Wen, X. Luo, C.-Y. Lee, X. Liu, X. Zhang, et al., A non-printed integrated-circuit textile for wireless theranostics, *Nature Communications* 12 (1) (2021) 4876.
- [65] H. Yousef, M. Boukallel, K. Althoefer, Tactile sensing for dexterous in-hand manipulation in robotics—A review, *Sensors and Actuators A: physical* 167 (2) (2011) 171–187.
- [66] Y. Yu, J. Li, S. A. Solomon, J. Min, J. Tu, W. Guo, C. Xu, Y. Song, W. Gao, All-printed soft human-machine interface for robotic physicochemical sensing, *Science Robotics* 7 (67) (2022) eabn0495.
- [67] W. Yuan, S. Dong, E. H. Adelson, Gelsight: High-resolution robot tactile sensors for estimating geometry and force, *Sensors* 17 (12) (2017) 2762.
- [68] Y. Zeng, T. E. Lee, J. Liang, O. Kroemer, Visual identification of articulated object parts, in: *IEEE/RSJ International Conference on Intelligent Robots and Systems (IROS)*, 2021.
- [69] H. Zhang, N. N. Chen, Control of contact via tactile sensing, *IEEE Transactions on Robotics and Automation (T-RA)* 16 (5) (2000) 482–495.
- [70] T. Zhang, Z. McCarthy, O. Jow, D. Lee, X. Chen, K. Goldberg, P. Abbeel, Deep imitation learning for complex manipulation tasks from virtual

- ality teleoperation, in: IEEE International Conference on Robotics and Automation (ICRA), 2018.
- [71] Z. Zhao, L. Cui, S. Xie, S. Zhang, Z. Han, L. Ruan, Y. Zhu, B*: Efficient and Optimal Base Placement for Fixed-Base Manipulators, arXiv preprint arXiv:2504.12719 .
- [72] Z. Zhao, W. Li, Y. Li, T. Liu, B. Li, M. Wang, K. Du, H. Liu, Y. Zhu, Q. Wang, et al., Embedding high-resolution touch across robotic hands enables adaptive human-like grasping, *Nature Machine Intelligence* 7 (6) (2025) 889–900.
- [73] Z. Zhao, Y. Li, W. Li, Z. Qi, L. Ruan, Y. Zhu, K. Althoefer, Tac-Man: Tactile-Informed Prior-Free Manipulation of Articulated Objects, *IEEE Transactions on Robotics (T-RO)* 41 (2024) 538–557.
- [74] B. Zheng, S. Verma, J. Zhou, I. W. Tsang, F. Chen, Imitation learning: Progress, taxonomies and challenges, *IEEE Transactions on Neural Networks and Learning Systems* 35 (99) (2022) 1–16.
- [75] Y. Zhu, T. Gao, L. Fan, S. Huang, M. Edmonds, H. Liu, F. Gao, C. Zhang, S. Qi, Y. N. Wu, et al., Dark, beyond deep: A paradigm shift to cognitive ai with humanlike common sense, *Engineering* 6 (3) (2020) 310–345.